Cerebellin-2 positive (*Cbln2*$^{+}$) Neurons in the Parafascicular Thalamic Nucleus Regulate Self-Grooming Behavior

Li Zhang[1*], Huimeng Song[2*], Yaning Li[3*], Huaxin Zhang[3*], Dandan Geng[3], Zijie Zhao[3], Bo Yang[3], Rong Zheng[3], Zekun Li[3], Lei Wang[3], Tianyun Zhang[3], Zhiyong Xie[4], Peng Cao[1#], Dapeng Li[2#], and Fan Zhang[3#]

[1] National Institute of Biological Sciences, Beijing, China. Tsinghua Institute of Multidisciplinary Biomedical Research, Tsinghua University, Beijing, China.

[2] School of Basic Medical Sciences, Laboratory for Clinical Medicine, Capital Medical University, Beijing, China.

[3] The Key Laboratory of Neural and Vascular Biology, Ministry of Education; The Key Laboratory of Vascular Biology of Hebei Province; Department of Biochemistry and Molecular Biology, Hebei Medical University, Shijiazhuang, China.

[4] Department of Psychological Medicine, Zhongshan Hospital, Institute for Translational Brain Research, State Key Laboratory of Medical Neurobiology, MOE Frontiers Center for Brain Science, MOE Innovative Center for New Drug Development of Immune Inflammatory Diseases, Fudan University, Shanghai, China

*These authors contributed equally

[#]Correspondence to:

caopeng@nibs.ac.cn

lidapeng2021@ccmu.edu.cn

zhangfan86@hebmu.edu.cn

Abstract

Self-grooming represents a stereotyped repetitive behavior which is commonly observed in various neuropsychiatric disorders. Deep brain stimulation (DBS) targeting the centromedian / parafascicular complex (CM/PF) has been shown to alleviate obsessive-compulsive disorder/behavior (OCD/OCB) symptoms in human. However, little is known about the neural circuits of the PF that are involved in the regulation of self-grooming behavior in rodents. Here, we report that *cerebellin-2* positive (*Cbln2*$^+$) neurons in PF bidirectionally encode self-grooming. Chemogenetic activation of *Cbln2*$^+$ PF neurons significantly reduces both physiological and pathological self-grooming, and chemogenetic inhibition of *Cbln2*$^+$ PF neurons increases physiological self-grooming. Moreover, activating synaptic excitatory inputs to *Cbln2*$^+$ PF neurons inhibits self-grooming, while synaptic inhibitory inputs enhance it. *Cbln2*$^+$ PF neurons independently transmit neural signals to the dorsal and ventral striatum. Activation of PF-dorsal striatum and PF-ventral striatum pathways both inhibit self-grooming behavior. Together, these data reveal that *Cbln2*$^+$ PF neurons are integral components of a brain network involved in self-grooming behavior.

Key Words

Self-grooming behavior; Parafascicular thalamic nucleus; *Cbln2*$^+$ neuron; Striatum; Neuropsychiatric disorders

INTRODUCTION

Self-grooming is an evolutionarily conserved behavior observed in arthropods (Lefebvre, 1981; Richard and Dawkins, 1976), birds (Lefebvre, 1982; Lefebvre and Joly, 1982; van RHIJN, 1977), and mammals (Berridge, 1990; Colonnese et al., 1996). In rodents, self-grooming has a complex sequenced structure that consists of repeated stereotyped movements, which follows an innate cephalo-caudal progression, preceding by a postural cephalo-caudal transition from paw - head grooming to body grooming (Kalueff et al., 2007; Kalueff et al., 2016). Humans also exhibit repetitive patterned behaviors including excoriation (skin-picking) (Ekore and Ekore, 2021; Lochner et al., 2017) and trichotillomania (hair-pulling) (Grant and Chamberlain, 2016; Hoffman et al., 2021; Stein et al., 2006), which are in analogy with the stereotyped repetitive self-grooming behavior in rodents and share several common traits and brain circuits with rodents (Grant and Chamberlain, 2016; Graybiel and Rauch, 2000; Robbins et al., 2019; Robertson, 2000; Stein et al., 2008). Repetitive patterned behaviors in human frequently occur in several neural neuropsychiatric diseases including autism spectrum disorder (ASD) (Sharma et al., 2018), Tourette syndrome (Robertson, 2000), and obsessive-compulsive disorder (OCD) (Goodman et al., 2021), making the grooming behavior in rodents ideal to study the neuropsychiatric disorders (Liu et al., 2020; Peça et al., 2011; Welch et al., 2007).

Excessive self-grooming is frequently observed in genetic animal models of neuropsychiatric disorders, including obsessive compulsive disorder/behavior (OCD/OCB) (Piantadosi et al., 2024; Xue et al., 2022), Tourette' syndrome (TS) (Liu et al., 2020), autism spectrum disorder (Peñagarikano et al., 2011; Silverman et al., 2010), and Rett syndrome (Chao et al., 2010; Gold et al., 2024). Thus, understanding the neural circuitry that regulates self-grooming could provide a new framework for the research of the development neuropsychiatric disorders.

The parafascicular thalamic (PF) nucleus in rodents, known as the counterpart of centromedian/ parafascicular complex (CM/PF) in primates, belongs to the intralaminar system of the thalamus (Langlois et al., 2010; Smith

et al., 2004). The PF nucleus play a role in limbic and associative network functions (Fallon et al., 2023; Lacey et al., 2007), and send glutamatergic projections to the striatum, which is involved in the completion of sequential syntactic self-grooming chains (Cromwell and Berridge, 1996; Zhang et al., 2022). Deep brain stimulation (DBS) targeting the CM/PF has been shown to alleviate obsessive-compulsive disorder/behavior (OCD/OCB) symptoms in human (Servello et al., 2020). However, it remains largely unknown whether PF nucleus have a critical role in the regulation of self-grooming in rodents.

In the present study, we combined genetically encoded circuit analysis tools to identify a subset of PF neurons critical for both biological and pathological self-grooming in mice. *Cbln2*$^{+}$ PF neurons bidirectionally encode self-grooming. Activating synaptic inhibitory inputs to *Cbln2*$^{+}$ PF neurons enhances self-grooming, while synaptic excitatory inputs inhibit it. Moreover, *Cbln2*$^{+}$ PF neurons regulate self-grooming behavior through both dorsal and ventral striatum. Our data reveal that *Cbln2*$^{+}$ PF neurons are integral components of a brain network involved in self-grooming behavior.

115 **RESULTS**

116

117 ***Cbln2*$^+$ PF neurons are required for the regulation of self-grooming**

118 At the beginning of this study, we measured self-grooming by using a
119 magnetic induction method (Inagaki et al., 2002; Xie et al., 2022) in parallel with
120 video recording, this was modified from the methods described in previous work
121 (Xie et al., 2022) (Fig. 1A). In previous study, the magnet was implanted in the
122 forelimb to track the movements of forelimb during orofacial grooming stage,
123 but it did not effectively indicate other types of grooming. Here, we implanted
124 the magnet on the surface of the skull to track the movements of head during
125 all types of self-grooming (Fig. 1A). The voltage threshold was calculated as
126 before (mean ± 5 × SD) and used to identify the voltage pulses corresponding
127 to the grooming behaviors. The magnetic inducing voltage signals efficiently
128 indicated the grooming behaviors in each stage, including paw-licking, orofacial
129 grooming and body grooming stage (Fig. 1B, and Movie S1). Then, we explored
130 the role of PF nucleus in mediating self-grooming. By using RNAscope analysis,
131 we found that the PF neurons are predominantly *Cbln2*$^+$ (more than 98% across
132 3 different sections, sFig.1A-B). To measure the contribution of *Cbln2*$^+$ PF
133 neurons to self-grooming, we injected AAV-DIO-ChR2-mCherry into the PF of
134 Cbln2-IRES-Cre mice, followed by optical fiber implantation above the PF
135 bilaterally (Fig. 1C). The effect of photostimulation to trigger action potential
136 firing in PF neurons expressing ChR2 was validated in acute brain slices (Fig.
137 1D). Optogenetic activation (473 nm, 10 s, 2 mW, 20 Hz) of *Cbln2*$^+$ PF neurons
138 significantly suppressed spontaneous self-grooming (sFig.1C-J), including
139 paw-licking (Fig. 1E), orofacial grooming (Fig. 1F), and body grooming (Fig. 1G)
140 in mice (Movie S2). Furthermore, optogenetic activation of *Cbln2*$^+$ PF neurons
141 also significantly suppressed oil-induced self-grooming (Xie et al., 2022) (Fig.
142 1H). These data suggested a preliminary conclusion that optogenetic activation
143 of *Cbln2*$^+$ PF neurons inhibit both spontaneous and oil-induced self-grooming.

144 Next, we injected AAV-DIO-hM3Dq-mCherry or AAV-DIO-hM4Di-mCherry
145 into the PF of Cbln2-IRES-Cre mice to verify the function of *Cbln2*$^+$ PF neurons

146 in regulation of grooming behavior within a long period (Fig. 1I, K). The effect
147 of CNO on chemogenetical modulation of action potential firing was validated
148 (Fig. 1J, L). We found that chemogenetic activation of *Cbln2*$^{+}$ PF neurons
149 significantly inhibited spontaneous self-grooming, including paw-licking (Fig.
150 1E), orofacial grooming (Fig. 1F), and body grooming (Fig. 1M and sFig.2B, D),
151 as well as oil-induced self-grooming (Fig. 1N), whereas chemogenetic inhibition
152 of these neurons enhanced both spontaneous and oil-induced self-grooming
153 (Fig. 1M-N and sFig.2C, D), suggesting that *Cbln2*$^{+}$ PF neurons regulate
154 grooming behavior in a bidirectional manner and potentially play key role in the
155 maintenance of balance in the grooming behavior. At the other hand,
156 chemogenetic activation of *Cbln2*$^{+}$ PF neurons caused slight reduction of total
157 distance, while chemogenetic inhibition of *Cbln2*$^{+}$ PF neurons showed no effect
158 on total locomotion distance (sFig.2A). Besides, optogenetic activation of
159 *Cbln2*$^{+}$ PF neurons also did not significantly change the total distance or
160 immobile time (sFig.1K, L), revealing that the regulation of *Cbln2*$^{+}$ PF neurons
161 on grooming behavior was not caused by the obvious motor system dysfunction.
162 The *Sapap3*-knockout (*Sapap3*$^{-/-}$) mouse is a model used to study OCD,
163 as it recapitulates OCD-like compulsive behavior through excessive grooming
164 (sFig.2E) (Hadjas et al., 2020; Welch et al., 2007). We surprisingly found that
165 chemogenetic activation of *Cbln2*$^{+}$ PF neurons also strongly inhibit pathological
166 self-grooming in *Sapap3*$^{-/-}$ mice (Fig. 1O). These data suggested that *Cbln2*$^{+}$
167 PF neurons are important components in the central circuit module that broadly
168 controls physiology and pathological self-grooming in mice.
169

170 **_Cbln2_$^{+}$ PF neurons encode self-grooming**

171 Next, we systematically characterized the physiological properties of
172 *Cbln2*$^{+}$ PF neurons. To assess the response properties of these neurons during
173 self-grooming, we recorded GCaMP signals in *Cbln2*$^{+}$ PF neurons using fiber
174 photometric recording. AAV-DIO-GCaMP7s was injected into the PF of Cbln2-
175 IRES-Cre mice, followed by implantation of an optical fiber above the *Cbln2*$^{+}$
176 PF neurons (Fig. 2A). Because the spontaneous grooming behavior does not

177 frequently occur, we sprayed the corn oil over the mice from head to toe to
178 induce more grooming behavior. In most trials, we found the mice exhibited
179 three major types of behaviors, including stationary state, locomotion and
180 grooming. GCaMP fluorescence of *Cbln2*$^{+}$ PF neurons during grooming was
181 higher than that of during stationary state, and lower than that of during
182 locomotion (sFig. 3A, B). Considering that the grooming behavior is a kind of
183 motor-related behavior, we chose to define the GCaMP fluorescence during the
184 period of locomotion as the baseline. These results lead to a conclusion that
185 *Cbln2*$^{+}$ PF neurons negatively regulate the grooming behavior, which is
186 consistent with the results that opotogenetic or chemogenetic activation of
187 *Cbln2*$^{+}$ PF inhibited grooming behavior.

188 In parallel with the oscillation of magnetic inducing voltage signal which
189 indicated the period of grooming, the GCaMP fluorescence of *Cbln2*$^{+}$ PF
190 neurons decreased immediately after the grooming behavior occurred, and
191 stayed fairly low until grooming stopped. (Fig. 2B) We also noticed that the
192 relative GCaMP fluorescence of *Cbln2*$^{+}$ PF showed negative correlation with
193 the grooming duration (grooming duration is defined as the duration of a bout,
194 pauses longer than 3 s constitute a new bout), suggesting that the *Cbln2*$^{+}$ PF
195 neurons might also be involved in the maintenance of grooming. (Fig. 2C).

196 To further analyze the temporal relationship between GCaMP signal and
197 self-grooming, we averaged the trials by aligning the GCaMP signal with the
198 exact time points of initiation or termination of self-grooming. The GCaMP
199 signal decreased immediately after the initiation of self-grooming (Fig. 2D-F).
200 We defined the offset time of GCaMP signal as the time when the signal
201 reaches 5% valley amplitude relative to the baseline. The average time when
202 GCaMP signal began to decrease was 329 ± 71 ms after the initiation of self-
203 grooming (Fig. 2G). The GCaMP signal began to recover to the baseline in prior
204 to the termination of self-grooming (Fig. 2H-J). We defined the onset time of
205 GCaMP signal as the time when the signal recovers to 95% valley amplitude
206 relative to the baseline. The average time when GCaMP signal began to rise
207 was 2531 ± 336 ms before the termination of self-grooming (Fig. 2K). These

208 results suggest that *Cbln2*$^+$ PF neurons are more likely involved in the initiation,
209 maintenance and termination of self-grooming.

210 To explore the neuronal activity of *Cbln2*$^+$ PF neurons at the single-cell
211 level, we performed in vivo calcium imaging by using the miniscope system on
212 free-moving mice (see methods for details, Fig. 2L). AAV-DIO-GCaMP7s was
213 injected into PF, followed by the implantation of a gradient refractive index
214 (GRIN) lens above the PF two weeks after viral injection (Fig. 2M). The example
215 coronal brain section revealed the site of GCaMP expression was restricted to
216 the PF, and the track of lens was exactly above the PF (Fig. 2N). In the trials
217 that recorded the initial stage of grooming (Movie S2), we detected three types
218 of GCaMP fluorescence response in *Cbln2*$^+$ PF neurons corresponding to the
219 grooming behavior (Fig. 2O, sFig. 3C). 75.00% of *Cbln2*$^+$ PF neurons (Type 1)
220 showed decreased response, 17.31% of *Cbln2*$^+$ PF neurons (Type 3) showed
221 increased response and 7.61% of *Cbln2*$^+$ PF neurons (Type 2) remained
222 unchanged (Fig. 2P), consistent with the results of fiber photometric recording
223 that the total response of GCaMP fluorescence was decreased during grooming
224 compared with that during baseline period (Fig. 2D-F). In the trials that recorded
225 the terminate stage of grooming (Movie S2), the GCaMP fluorescence
226 response in *Cbln2*$^+$ PF neurons could also be classified into three types (Fig.
227 2Q, sFig. 3D). Most of the *Cbln2*$^+$ PF neurons (70.51%, Type 1) showed
228 increased response, 16.03% of *Cbln2*$^+$ PF neurons (Type 3) showed deceased
229 response and 13.46% of *Cbln2*$^+$ PF neurons (Type 2) remained unchanged
230 when the grooming behavior terminated (Fig. 2R), which was also consistent
231 with the results of fiber photometric recording which recorded the terminate
232 stage of grooming (Fig. 2H-J). Together, these data further confirmed the
233 conclusion that *Cbln2*$^+$ PF neurons play a negative role in the regulation of self-
234 grooming.

235

236 **Mapping the monosynaptic inputs of *Cbln2*$^+$ PF neurons**

237 Using recombinant rabies virus, we next performed monosynaptic
238 retrograde tracing (Wickersham et al., 2007) to examine how *Cbln2*$^+$ PF

239 neurons are connected to brain areas associated with self-grooming (Fig. 3A–
240 C). A brain-wide survey revealed a series of monosynaptic projections to the
241 *Cbln2*$^+$ PF neurons (Fig. 3D, E). Among these brain regions, we focused on the
242 brain regions such as superior colliculus (SC), substantia nigra pars reticulata
243 (SNr), zona incerta (ZI) and lateral parabrachial nucleus (LPB). First, robust
244 monosynaptic inputs arose from SC (Fig. 3D2). Prenatal or early postnatal
245 factors could disrupt SC functions, thus resulting in autism (Jure, 2019; Liu et
246 al., 2022), which was reported to show excessive grooming behavior in rodents
247 (Peça et al., 2011). Second, *Cbln2*$^+$ PF neurons were monosynaptically
248 innervated by neurons in ZI and SNr (Fig. 3D3, D4), two brain areas that are
249 involved in the self-grooming behavior in mice (Jiang et al., 2024; Meyer-
250 Luehmann et al., 2002). Third, *Cbln2*$^+$ PF neurons were also innervated by
251 neurons in LPB (Fig. 3D1). Previous study showed that LPB glutamatergic (Glu)
252 neurons were involved in stress-induced self-grooming (Jia et al., 2023). These
253 data supported the hypothesis that *Cbln2*$^+$ PF neurons are within a brain
254 network for self-grooming behavior.
255

256 **Multiple *Cbln2*$^+$ PF neurons input pathways involved in self-grooming**

257 Next, we tested whether projections from multiple brain regions to *Cbln2*$^+$
258 PF neurons were involved in the regulation of self-grooming. We injected AAV-
259 DIO-hM3Dq-mCherry into the SC (Fig. 4A, B) or LPB (Fig. 4E, F) of vGluT2-
260 IRES-Cre mice, which followed by cannulae implantation above the PF (Fig.
261 4C, G). By the perfusion of CNO into the PF through the cannulae, the vGluT2$^+$
262 SC or LPB-PF pathway was activated. We found that chemogenetic activation
263 of either vGlut2$^+$ SC-PF pathway (Fig. 4D) or vGlut2$^+$ LPB-PF pathway (Fig. 4H)
264 significantly inhibited spontaneous self-grooming, including paw-licking,
265 orofacial grooming, and body grooming in mice (sFig. 4B, C). Then, we injected
266 AAV-DIO-hM3Dq-mCherry into the SNr (Fig. 4I, J) or ZI (Fig. 4M, N) of vGAT-
267 IRES-Cre mice, which followed by cannulae implantation above the PF (Fig. 4K,
268 O). We found that chemogenetic activation of either vGAT$^+$ SC-PF pathway (Fig.
269 4L) or vGAT$^+$ ZI-PF pathway (Fig. 4P) significantly facilitated spontanous self-

270 grooming, including paw-licking, orofacial grooming, and body grooming in
271 mice (sFig. 4D, E). These results verified the inhibitory role of the glutamatergic
272 inputs from SC or LPB to *Cbln2*$^+$ PF neurons and the excitatory role of the
273 GABAergic inputs from SNr or ZI to *Cbln2*$^+$ PF neurons on grooming behavior,
274 further elucidating that *Cbln2*$^+$ PF neurons are within a complex brain network
275 and bidirectionally regulate grooming behavior.
276

277 **The *Cbln2*$^+$ PF–striatum pathway is required for self-grooming**

278 Next, we injected AAV-DIO-EGFP into the PF of Cbln2-IRES-Cre mice to
279 map the efferent pathways of *Cbln2*$^+$ PF neurons involved in the grooming
280 behavior. (Fig. 5A-B). We found that the *Cbln2*$^+$ PF neurons divergently
281 projected to various brain regions, including the dorsal striatum (CPu), and the
282 ventral striatum (aca, AcbC and Tu). (Fig. 5C), and other brain regions (sFig.
283 5A-H). We tested the striatum as the possible relay station mediating PF-related
284 grooming behavior as following reasons: first, the activity of striatal cells is
285 reported to be orchestrated to represent the important timepoints in a grooming
286 sequence (Minkowicz et al., 2023); second, striatal dysfunction and defects in
287 cortico-striatal function have been observed in repetitive and compulsive
288 grooming behaviors in autism model mice (Peça et al., 2011) and striatal-
289 specific expression of *Sapap3* rescues the over-grooming behavior in OCD
290 mice (Welch et al., 2007); third, ventral capsule/ventral striatum DBS
291 significantly reduced OCD symptoms in human (Graat et al., 2017; Welter et al.,
292 2021).

293 The striatum, consisting of dorsal and ventral part, receives inputs from
294 distinct subpopulations of neurons in PF (Zhang et al., 2022). The ventral part
295 of the striatum and the ventral striatal islands of Calleja were particularly
296 reported to be involved in the regulation of grooming behavior in rodents (Xue
297 et al., 2022; Zhang et al., 2021), however, function of the dorsal part of striatum
298 in grooming behavior was poorly elucidated. Hence it is essential to verify if PF
299 regulates grooming behavior through two distinct PF-striatum pathways.

300 By using the strategy of retrograde labeling of cholera toxin subunit B (CTB)

301 and wheat germ agglutinin (WGA) (Fig. 5D), we labelled PF neurons which sent
302 projections to the dorsal striatum and the ventral striatum (Fig. 5E). The dorsal
303 striatum-projecting PF neurons and ventral striatum-projecting PF neurons
304 were scarcely overlapped (double labelled neurons were no more than 1.5%)
305 in spatial arrangement (Fig. 5F-I). It would be essential to clarify the role of
306 these two distinct pathways in PF-mediating grooming behavior regulation.

307 Therefore, we injected AAV-DIO-hM3Dq-mCherry into the PF of Cbln2-
308 IRES-Cre mice (Fig. 5J, K, N, O), which followed by cannulae implantation
309 above the dorsal striatum (Fig. 5L) or ventral striatum (Fig. 5P). We found that
310 chemogenetic activation of either *Cbln2*$^{+}$ PF-dorsal striatum pathway (Fig. 5M)
311 or *Cbln2*$^{+}$ PF-ventral striatum pathway (Fig. 4H) significantly inhibited
312 spontaneous self-grooming, including paw-licking, orofacial grooming, and
313 body grooming in mice (sFig. 4F, G). Together, these data elucidated the pivotal
314 role of both the dorsal striatum and ventral striatum in the regulation of PF-
315 mediating grooming regulation.

316 In addition to the majority of GABAergic spiny projection neurons, there are
317 many kinds of interneurons in the striatum, which act on nearby circuits and
318 shape functional output to the basal ganglia (Muñoz-Manchado et al., 2018).
319 By the injection of AAV-DIO-EGFP-Syb2 into the PF of Cbln2-IRES-Cre mice
320 (sFig.5I), we found that the striatal cells positive for PV, SST, ChAT and NPY in
321 both the dorsal striatum and ventral striatum were surrounded by the synaptic
322 terminals from *Cbln2*$^{+}$ PF neurons (sFig.5J, K), which offered putative targets
323 to divergently regulate the grooming behavior. However, further work was
324 essential to elucidate the functional connections between *Cbln2*$^{+}$ PF neurons
325 and these striatal cells and the role of these striatal cells in grooming regulation
326 under the innervation of *Cbln2*$^{+}$ PF neurons.
327

DISCUSSION

Self-grooming is an innate behavior with important physiological functions including hygiene maintenance, thermoregulation, social communication (Kalueff et al., 2016; Leonard et al., 2005; Spruijt et al., 1992). Recently, the repetitive stereotyped behavior of mice was reported to cope with stress and post-stress anxiety alleviation (Sun et al., 2022). In this study, we identified that *Cbln2*$^+$ PF neurons encode self-grooming in a bidirectional manner. Synaptic excitatory inputs that activate *Cbln2*$^+$ PF neurons inhibit spontaneous self-grooming, and synaptic inhibitory inputs enhance it. Moreover, *Cbln2*$^+$ PF neurons regulate self-grooming behavior through both dorsal and ventral striatum. Together, these data elucidate that *Cbln2*$^+$ PF neurons are a central component of a brain network involved in self-grooming behavior.

Our data also showed that chemogenetic activation of *Cbln2*$^+$ PF neurons substantially decreased the excessive pathological self-grooming in OCD mice (Welch et al., 2007), providing a solid neurobiological foundation for the improvement of OCD/OCB symptoms under the treatment of DBS in PF in human (Servello et al., 2020).

The PF nucleus participates in sensorimotor coordination (Liu et al., 2008), pain and nociception (Sims-Williams et al., 2016; Weigel and Krauss, 2004). Sensory perception is one of the cases inducing grooming behavior (Xie et al., 2022). Among the brain regions we mapped which send inputs to PF, SC and LPB are reported to mediate the circuits of sensory perception (Choi et al., 2023; Nagashima et al., 2023), and ZI is believed to have many integrative functions that link sensory stimuli with motor responses to guide behavior (Hormigo et al., 2023). Optogenetic and chemogenetic activation of *Cbln2*$^+$ PF neurons inhibit the oil-induced self-grooming, reveal the importance of the PF nucleus in sensory-induced grooming behavior, while may also suggest that the PF nucleus is broadly involved in the regulation of grooming behavior within a complex neural network.

Cbln2$^+$ PF neurons send projections to various brain regions, including the dorsal striatum, the ventral striatum and others. Here we have proven that PF-dorsal striatum pathway and PF-ventral striatum pathway are spatially

independent but both involved in self-grooming regulation, specifying the effect of dorsal striatum on grooming behavior which was rarely reported in rodents. Besides the striatum receiving outputs from *Cbln2*$^{+}$ PF neurons, the periaqueductal gray (PAG) and the ventral tegmental area (VTA) are also potentially innervated by *Cbln2*$^{+}$ PF neurons and reported to implicate in grooming behavior (Gao et al., 2019; Sun et al., 2022). In future studies, it would be important to examine whether these two brain regions are involved in PF-mediating grooming regulation, thereby enriches the landscape of research on the regulation of grooming behavior.

There are certain limitations in our present study. First, the magnetic inducing voltage signals induced by embedding a magnet in the head only provide a relatively more comprehensive reflection of grooming behavior. However, further analysis on the characteristics of the voltage signals corresponding to different types of grooming will be helpful to automatically distinguish among them. Second, *Cbln2* is expressed in the vast majority of PF neurons, with the proportion exceeding 98%. Our miniscope data revealed three types of neurons with different responses to grooming behavior, addressing the question that classification of detailed subtypes of neurons in PF nucleus combining with single-cell sequence would be necessary to better elucidate how PF neurons encode self-grooming. Third, chemogenetic activation of *Cbln2*$^{+}$ PF neurons significantly alleviated the excessive grooming in OCD mice, while further electrophysiological, structural and biochemical studies are essential to refine the neural mechanism of *Cbln2*$^{+}$ PF neurons on pathological grooming regulation, which would prospectively bring new therapeutic target for OCD.

Acknowledgments

This work was supported by STI 2030-Major Projects [Grant 2021ZD 0203200-04 (to F.Z.)], National Natural Science Foundation of China [Grant 32171018 (to F.Z.), Grant 32271030 (to D.L.)], Natural Science Foundation of Hebei Province [Grant H2022206011 (to F.Z.), C2024206032 (to F.Z.)], Top Talent of Young People of Hebei Province (to F.Z.).

Author contributions

Conceptualization, P.C., F.Z., and L.Z.; methodology, D.L.; investigation, D.G., Y.L., Z.L., H.S., L.W., Z. X., B.Y., L.Z., R.Z., T.Z., and Z.Z.; writing– original draft, P.C., F.Z., and L.Z.; funding acquisition, D.L. and F.Z.; resources, P.C., D.L. and F.Z.; supervision, P.C., F.Z., and L.Z.

References

Berridge, K.C. (1990). Comparative fine structure of action: Rules of form and sequence in the grooming patterns of six rodent species. Behaviour 113, 21-56.

Chao, H.T., Chen, H., Samaco, R.C., Xue, M., Chahrour, M., Yoo, J., Neul, J.L., Gong, S., Lu, H.C., Heintz, N., et al. (2010). Dysfunction in GABA signalling mediates autism-like stereotypies and Rett syndrome phenotypes. Nature 468, 263-269.

Choi, J.S., Ayupe, A.C., Beckedorff, F., Catanuto, P., McCartan, R., Levay, K., and Park, K.K. (2023). Single-nucleus RNA sequencing of developing superior colliculus identifies neuronal diversity and candidate mediators of circuit assembly. Cell Rep. 42, 113037.

Colonnese, M.T., Stallman, E.L., and Berridge, K.C. (1996). Ontogeny of Action Syntax in Altricial and Precocial Rodents: Grooming Sequences of Rat and Guinea Pig Pups. Behaviour 133, 1165-1195.

Cromwell, H.C., and Berridge, K.C. (1996). Implementation of Action Sequences by a Neostriatal Site: A Lesion Mapping Study of Grooming Syntax. J. Neurosci. 16, 3444-3458.

Ekore, R.I., and Ekore, J.O. (2021). Excoriation (skin-picking) disorder among adolescents and young adults with acne-induced postinflammatory hyperpigmentation and scars. Int. J. Dermatol. 60, 1488-1493.

Fallon, I.P., Hughes, R.N., Ulloa Severino, F.P., Kim, N., Lawry, C.M., Watson, G.D.R., Roshchina, M., and Yin, H.H. (2023). The role of the parafascicular thalamic nucleus in action initiation and steering. Curr. Biol. 33, 2941-2951.e2944.

Gao, Z.R., Chen, W.Z., Liu, M.Z., Chen, X.J., Wan, L., Zhang, X.Y., Yuan, L., Lin, J.K., Wang, M., Zhou, L., et al. (2019). Tac1-Expressing Neurons in the Periaqueductal Gray Facilitate the Itch-Scratching Cycle via Descending Regulation. Neuron 101, 45-59.e49.

Gold, W.A., Percy, A.K., Neul, J.L., Cobb, S.R., Pozzo-Miller, L., Issar, J.K., Ben-Zeev, B., Vignoli, A., and Kaufmann, W.E. (2024). Rett syndrome. Nat. Rev. Dis. Primers 10, 84.

Goodman, W.K., Storch, E.A., and Sheth, S.A. (2021). Harmonizing the Neurobiology and Treatment of Obsessive-Compulsive Disorder. Am. J. Psychiatry 178, 17-29.

Graat, I., Figee, M., and Denys, D. (2017). The application of deep brain stimulation in the treatment of psychiatric disorders. Int. Rev. Psychiatry 29, 178-190.

Grant, J.E., and Chamberlain, S.R. (2016). Trichotillomania. Am. J. Psychiatry 173, 868-874.

Graybiel, A.M., and Rauch, S.L. (2000). Toward a Neurobiology of Obsessive-Compulsive Disorder. Neuron 28, 343-347.

Hadjas, L.C., Schartner, M.M., Cand, J., Creed, M.C., Pascoli, V., Lüscher, C., and Simmler, L.D. (2020). Projection-specific deficits in synaptic transmission

in adult Sapap3-knockout mice. Neuropsychopharmacology 45, 2020-2029.
Hoffman, J., Williams, T., Rothbart, R., Ipser, J.C., Fineberg, N., Chamberlain, S.R., and Stein, D.J. (2021). Pharmacotherapy for trichotillomania. Cochrane Database Syst. Rev.
Hormigo, S., Zhou, J., Chabbert, D., Sajid, S., Busel, N., and Castro-Alamancos, M. (2023). Zona incerta distributes a broad movement signal that modulates behavior. eLife 12, RP89366.
Inagaki, N., Igeta, K., Kim, J.F., Nagao, M., Shiraishi, N., Nakamura, N., and Nagai, H. (2002). Involvement of unique mechanisms in the induction of scratching behavior in BALB/c mice by compound 48/80. Eur. J. Pharmacol. 448, 175-183.
Jia, T., Chen, J., Wang, Y., Xiao, C., and Zhou, C. (2023). A subthalamo-parabrachial glutamatergic pathway is involved in stress-induced self-grooming in mice. Acta Pharmacol. Sin. 44, 2169-2183.
Jiang, Z., He, M., Young, C., Cai, J., Xu, Y., Jiang, Y., Li, H., Yang, M., and Tong, Q. (2024). Dopaminergic Neurons in Zona Incerta Drives Appetitive Self-Grooming. Adv. Sci. 11, 2308974.
Jure, R. (2019). Autism Pathogenesis: The Superior Colliculus. Front. Neurosci. 12.
Kalueff, A.V., Aldridge, J.W., LaPorte, J.L., Murphy, D.L., and Tuohimaa, P. (2007). Analyzing grooming microstructure in neurobehavioral experiments. Nat. Protoc. 2, 2538-2544.
Kalueff, A.V., Stewart, A.M., Song, C., Berridge, K.C., Graybiel, A.M., and Fentress, J.C. (2016). Neurobiology of rodent self-grooming and its value for translational neuroscience. Nat. Rev. Neurosci. 17, 45-59.
Lacey, C.J., Bolam, J.P., and Magill, P.J. (2007). Novel and Distinct Operational Principles of Intralaminar Thalamic Neurons and Their Striatal Projections. J. Neurosci. 27, 4374-4384.
Langlois, M., Polack, P.O., Bernard, H., David, O., Charpier, S., Depaulis, A., and Deransart, C. (2010). Involvement of the Thalamic Parafascicular Nucleus in Mesial Temporal Lobe Epilepsy. J. Neurosci. 30, 16523-16535.
Lefebvre, L. (1981). Grooming in crickets: Timing and hierarchical organization. Anim. Behav. 29, 973-984.
Lefebvre, L. (1982). The organization of grooming in budgerigars. Behav. Processes 7, 93-106.
Lefebvre, L., and Joly, R. (1982). Organization rules and timing in kestrel grooming. Anim. Behav. 30, 1020-1028.
Leonard, S.T., Alizadeh-Naderi, R., Stokes, K., and Ferkin, M.H. (2005). The role of prolactin and testosterone in mediating seasonal differences in the self-grooming behavior of male meadow voles, Microtus pennsylvanicus. Physiol. Behav. 85, 461-468.
Liu, C., Wang, Y., Smallwood, P.M., and Nathans, J. (2008). An Essential Role for Frizzled5 in Neuronal Survival in the Parafascicular Nucleus of the Thalamus. J. Neurosci. 28, 5641-5653.

Liu, S., Tian, M., He, F., Li, J., Xie, H., Liu, W., Zhang, Y., Zhang, R., Yi, M., Che, F., et al. (2020). Mutations in ASH1L confer susceptibility to Tourette syndrome. Mol. Psychiatry 25, 476-490.
Liu, X., Huang, H., Snutch, T.P., Cao, P., Wang, L., and Wang, F. (2022). The Superior Colliculus: Cell Types, Connectivity, and Behavior. Neurosci. Bull. 38, 1519-1540.
Lochner, C., Roos, A., and Stein, D.J. (2017). Excoriation (skin-picking) disorder: a systematic review of treatment options. Neuropsychiatr. Dis. Treat. 13, 1867-1872.
Meyer-Luehmann, M., Thompson, J.F., Berridge, K.C., and Aldridge, J.W. (2002). Substantia nigra pars reticulata neurons code initiation of a serial pattern: implications for natural action sequences and sequential disorders. Eur. J. Neurosci. 16, 1599-1608.
Muñoz-Manchado, A.B., Bengtsson Gonzales, C., Zeisel, A., Munguba, H., Bekkouche, B., Skene, N.G., Lönnerberg, P., Ryge, J., Harris, K.D., Linnarsson, S., et al. (2018). Diversity of Interneurons in the Dorsal Striatum Revealed by Single-Cell RNA Sequencing and PatchSeq. Cell Rep. 24, 2179-2190.e2177.
Nagashima, T., Mikami, K., Tohyama, S., Konno, A., Hirai, H., and Watabe, A.M. (2023). State-dependent modulation of positive and negative affective valences by a parabrachial nucleus-to-ventral tegmental area pathway in mice. Front. Neural Circuits 17.
Peça, J., Feliciano, C., Ting, J.T., Wang, W., Wells, M.F., Venkatraman, T.N., Lascola, C.D., Fu, Z., and Feng, G. (2011). Shank3 mutant mice display autistic-like behaviours and striatal dysfunction. Nature 472, 437-442.
Peñagarikano, O., Abrahams, Brett S., Herman, Edward I., Winden, Kellen D., Gdalyahu, A., Dong, H., Sonnenblick, Lisa I., Gruver, R., Almajano, J., Bragin, A., et al. (2011). Absence of CNTNAP2 Leads to Epilepsy, Neuronal Migration Abnormalities, and Core Autism-Related Deficits. Cell 147, 235-246.
Piantadosi, S.C., Manning, E.E., Chamberlain, B.L., Hyde, J., LaPalombara, Z., Bannon, N.M., Pierson, J.L., K Namboodiri, V.M., and Ahmari, S.E. (2024). Hyperactivity of indirect pathway-projecting spiny projection neurons promotes compulsive behavior. Nat. Commun. 15, 4434.
Richard, and Dawkins, M. (1976). Hierachical organization and postural facilitation: Rules for grooming in flies. Anim. Behav. 24, 739-755.
Robbins, T.W., Vaghi, M.M., and Banca, P. (2019). Obsessive-Compulsive Disorder: Puzzles and Prospects. Neuron 102, 27-47.
Robertson, M.M. (2000). Tourette syndrome, associated conditions and the complexities of treatment. Brain 123 Pt 3, 425-462.
Servello, D., Galbiati, T.F., Balestrino, R., Iess, G., Zekaj, E., De Michele, S., and Porta, M. (2020). Deep Brain Stimulation for Gilles de la Tourette Syndrome: Toward Limbic Targets. Brain Sci. 10, 301.
Sharma, S.R., Gonda, X., and Tarazi, F.I. (2018). Autism Spectrum Disorder: Classification, diagnosis and therapy. Pharmacol. Ther. 190, 91-104.
Silverman, J.L., Tolu, S.S., Barkan, C.L., and Crawley, J.N. (2010). Repetitive

533 Self-Grooming Behavior in the BTBR Mouse Model of Autism is Blocked by the
534 mGluR5 Antagonist MPEP. Neuropsychopharmacology 35, 976-989.
535 Sims-Williams, H.P., Javed, S., Pickering, A.E., and Patel, N.K. (2016).
536 Characterising the Analgesic Effect of Different Targets for Deep Brain
537 Stimulation in Trigeminal Anaesthesia Dolorosa. Stereotact. Funct. Neurosurg.
538 94, 174-181.
539 Smith, Y., Raju, D.V., Pare, J.F., and Sidibe, M. (2004). The thalamostriatal
540 system: a highly specific network of the basal ganglia circuitry. Trends Neurosci.
541 27, 520-527.
542 Spruijt, B.M., van Hooff, J.A., and Gispen, W.H. (1992). Ethology and
543 neurobiology of grooming behavior. Physiol. Rev. 72, 825-852.
544 Stein, D.J., Chamberlain, S.R., and Fineberg, N. (2006). An A-B-C Model of
545 Habit Disorders: Hair-Pulling, Skin-Picking, and Other Stereotypic Conditions.
546 CNS Spectrums 11, 824-827.
547 Stein, D.J., Flessner, C.A., Franklin, M., Keuthen, N.J., Lochner, C., and Woods,
548 D.W. (2008). Is trichotillomania a stereotypic movement disorder? An analysis
549 of body-focused repetitive behaviors in people with hair-pulling. Ann. Clin.
550 Psychiatry 20, 194-198.
551 Sun, J., Yuan, Y., Wu, X., Liu, A., Wang, J., Yang, S., Liu, B., Kong, Y., Wang,
552 L., Zhang, K., et al. (2022). Excitatory SST neurons in the medial paralemniscal
553 nucleus control repetitive self-grooming and encode reward. Neuron 110, 3356-
554 3373.e3358.
555 van RHIJN, J.G. (1977). The Patterning of Preening and Other Comfort
556 Behaviour in a Herring Gull. Behaviour 63, 71-109.
557 Weigel, R., and Krauss, J.K. (2004). Center Median-Parafascicular Complex
558 and Pain Control: Review from a Neurosurgical Perspective. Stereotact. Funct.
559 Neurosurg. 82, 115-126.
560 Welch, J.M., Lu, J., Rodriguiz, R.M., Trotta, N.C., Peca, J., Ding, J.D., Feliciano,
561 C., Chen, M., Adams, J.P., Luo, J., et al. (2007). Cortico-striatal synaptic defects
562 and OCD-like behaviours in Sapap3-mutant mice. Nature 448, 894-900.
563 Welter, M.L., Alves Dos Santos, J.F., Clair, A.H., Lau, B., Diallo, H.M.,
564 Fernandez-Vidal, S., Belaid, H., Pelissolo, A., Domenech, P., Karachi, C., et al.
565 (2021). Deep Brain Stimulation of the Subthalamic, Accumbens, or Caudate
566 Nuclei for Patients With Severe Obsessive-Compulsive Disorder: A
567 Randomized Crossover Controlled Study. Biol. Psychiatry 90, e45-e47.
568 Wickersham, I.R., Finke, S., Conzelmann, K.K., and Callaway, E.M. (2007).
569 Retrograde neuronal tracing with a deletion-mutant rabies virus. Nat. Methods
570 4, 47-49.
571 Xie, Z., Li, D., Cheng, X., Pei, Q., Gu, H., Tao, T., Huang, M., Shang, C., Geng,
572 D., Zhao, M., et al. (2022). A brain-to-spinal sensorimotor loop for repetitive self-
573 grooming. Neuron 110, 874-890.e877.
574 Xue, J., Qian, D., Zhang, B., Yang, J., Li, W., Bao, Y., Qiu, S., Fu, Y., Wang, S.,
575 Yuan, T., et al. (2022). Midbrain dopamine neurons arbiter OCD-like behavior.
576 Proc. Natl. Acad. Sci. 119, e2207545119.

Zhang, Y., Roy, D.S., Zhu, Y., Chen, Y., Aida, T., Hou, Y., Shen, C., Lea, N.E., Schroeder, M.E., Skaggs, K.M., et al. (2022). Targeting thalamic circuits rescues motor and mood deficits in PD mice. Nature 607, 321-329.

Zhang, Y.F., Vargas Cifuentes, L., Wright, K.N., Bhattarai, J.P., Mohrhardt, J., Fleck, D., Janke, E., Jiang, C., Cranfill, S.L., Goldstein, N., et al. (2021). Ventral striatal islands of Calleja neurons control grooming in mice. Nat. Neurosci. 24, 1699-1710.

585 **Methods**

586

587 **Animals.** All the mice-using experimental procedures were conducted following
588 the protocols approved by the Administrative Panel on Laboratory Animal Care
589 in the National Institute of Biological Sciences (NIBS) in Beijing, China. Mouse
590 lines used in this study, including vGluT2-Cre and VGAT-Cre were imported
591 from the Jackson Laboratory (JAX Mice and Services). Cbln2-IRES-Cre mice
592 were generated in NIBS and Sapap3$^{-/-}$ mice were purchased from the
593 GemPharmatech Co., Ltd. Mice were housed in groups (3-5 animals per cage)
594 and maintained under a 12-h light/12-h dark cycle with food and water available
595 *ad libitum*. Mice were separated 3 days before virus injection and housed
596 individually after virus injection until subsequent experiments were conducted.
597 Only male mice were used to avoid potential sexual divergence. Primers used
598 for genotyping are listed in Supplementary Table 2.

599

600 **AAV vectors.** Viral particles used in this study were purchased from Shanghai
601 Taitool Bioscience Inc., BrainVTA Inc. and OBiO Technology Inc. Detailed
602 information about the AAVs were listed in the Supplementary Table 2. The final
603 titer used for AAV injection was 5×10^{12} viral particles/ml.

604

605 **Stereotaxic injection.** Mice were anesthetized with an intraperitoneal injection
606 of tribromoethanol (125-250 mg per kg). Standard surgery was performed to
607 expose the brain surface above the target brain regions, including PF, SC, LPB,
608 ZI, SNr, dorsal striatum and ventral straitum. Coordinates used to inject PF were
609 as follows: bregma -2.30 mm, lateral ±0.65 mm and dura -3.20 mm.
610 Coordinates used to inject SC were as follows: bregma -3.80 mm, lateral ±1.20
611 mm and dura -1.55 mm. Coordinates used for LPB injection were as follows:
612 bregma -5.43 mm, lateral ±1.35 mm and bregma -3.50 mm. Coordinates used
613 for ZI injection were as follows: bregma -1.79 mm, lateral ±1.28 mm and dura -
614 4.09 mm. Coordinates used for SNr injection were as follows: bregma -3.13 mm,
615 lateral ±1.37 mm and dura -4.36 mm. Coordinates used for dorsal striatum
616 injection were as follows: bregma +0.86 mm, lateral ±1.70 mm and dura -2.60

617 mm. Coordinates used for ventral striatum injection were as follows: bregma
618 +1.20 mm, lateral ±1.50 mm and dura -4.45 mm. The AAVs, CTB-488 and
619 WGA-555 were stereotaxically injected using a glass pipette connected to a
620 Nanoliter-Injector 201 (World Precision Instruments) at a slow flow rate of 0.15
621 μl min^{-1} to avoid potential damage to local brain tissue. The pipette was
622 withdrawn at least 20 min after viral injection.
623 For optogenetic activation, AAV injections were bilateral. For chemogenetic
624 activation/inactivation, injections were bilateral. For chemogenetically synaptic
625 activation, injections were bilateral. Behavioral tests were conducted 3 weeks
626 after viral injection. Slice physiology and histology were conducted at least 3
627 weeks after AAV injection.
628
629 **Optical fiber implantation.** Thirty minutes after AAV injection, a ceramic ferrule
630 with an optical fiber (for optogenetics: 200 μm in diameter, numerical aperture
631 (NA) of 0.37; for fiber photometric recording: 200 μm in diameter, NA of 0.37)
632 was implanted with the fiber tip on top of the PF (bregma -2.30 mm, lateral ±
633 1.71 mm and bregma -2.55 mm with a 20° angle towards the midline). The
634 ferrule was then secured onto the skull with dental cement. After implantation,
635 the antibiotics were applied to the surgical wound. The optogenetic and fiber
636 photometric recording experiments were conducted 3 weeks after the optical
637 fiber implantation. For optogenetic stimulation, the output of the laser was
638 measured and adjusted to various intensities of 2 mW or 0.2 mW before each
639 experiment. The pulse onset, duration, and frequency of light stimulation were
640 controlled by a programmable pulse generator attached to the laser system.
641
642 **Cannula implantation and drug infusion.** Two cannulae were bilaterally
643 implanted above the PF, dorsal striatum or ventral striatum regions. The inner
644 and outer diameters of the cannula were 150 μm and 300 μm, respectively.
645 Each cannula was fixed to the skull with dental cement. During drug infusion,
646 each cannula was connected with a catheter filled with CNO (3 μM) or saline
647 for injection. The other side of the catheter was connected to a Hamilton syringe

648 controlled by an infusion pump to drive the delivery of CNO or saline (50 nl
649 min−1). The catheter was removed 5 minutes after the delivery of CNO or saline
650 was completed. Then the mice were back to homecage for a 30-minute rest
651 and used for the subsequent behavior tests. At the end of the experimental
652 session, the test mice were perfused, and the coronal brain sections containing
653 PF, dorsal striatum or ventral striatum regions were inspected for the presence
654 of cannula track. The mice with no cannula track above the PF, dorsal striatum
655 or ventral striatum were rejected from further analysis.
656
657 **Preparation of behavioral tests.** After AAV injection and fiber implantation,
658 the mice were housed individually for 3 weeks, and handled daily by the
659 experimenters for at least 3 days before the behavioral tests. On the day of the
660 behavioral test, the mice were transferred to the testing room and were
661 habituated to the room conditions for 3 h before the experiments started. The
662 apparatus was cleaned with 20% ethanol, to eliminate odor cues from other
663 mice. All behavioral tests were conducted during the same circadian period
664 (13:00–19:00). All behaviors were scored by the experimenters, who were
665 blinded to the animal treatments.
666
667 **Magnetic induction to record head movements during self-grooming.** The
668 magnetic induction system to measure self-grooming was constructed in the
669 light of a magnetic induction system to measure scratching behavior (Inagaki
670 et al., 2002). For the mice without fibers or cannulae, a small skin cut (1 mm)
671 was made in the scalp under anesthesia. A metal guide tube with sharp tip that
672 carried a magnet cylinder (1 mm in diameter, 3 mm in length) was inserted
673 subcutaneously. Then the cylinder was pulled out, while leaving the magnet
674 inside the scalp. A drop of vet glue was applied to help the skin cut sealed well
675 and healed. The mice could be tested 3 days after the surgery. For the mice
676 with fibers or cannulae, the magnet cylinder was placed on the skull and
677 wrapped in dental cement during the surgery of fiber/cannula implantation.
678 Then the behavior tests were conducted 3 weeks after the surgery.

679 The tested mouse was placed in the chamber in a Helmholtz coil (230 mm in
680 diameter, CTXQ-230, Li Tian magnetoelectric Technology Inc.), or in the arena
681 above a Helmholtz coil. The electric potential induced in the coil by the
682 movement of magnets was amplified (100x) and recorded with Spike2 software
683 (CED Inc., UK). In Spike2 software, the raw electrical potential data was
684 removed DC offset, passed through a digital low pass filter (Butterworth, fourth
685 order, corner: 40 Hz) and smoothed (time constant: 0.04 s). The mean voltage
686 of when the mice were stationary was calculated as the baseline. The threshold
687 to identify the head movement during self-grooming was defined as the mean
688 voltage of baseline plus 5 × SD (standard deviation).
689
690 **Recording the time spent for spontaneous self-grooming and oil-induced**
691 **self-grooming.** On the day of experiment, the test mouse was allowed to
692 explore a cylinder (15 cm in diameter) for 15 minutes. For oil-induced grooming,
693 the experimenter sprayed corn oil on the test mice from the top of the cylinder
694 to make the mice covered with a thin layer of oil after the freely exploration in
695 the cylinder. The behavior of self-grooming was identified by both visual
696 inspection and the magnetic induction trace reflecting the rhythmic head
697 movements. The oil-induced self-grooming was quantified by measuring the
698 time spent for self-grooming during the 30 minutes after the spray of oil onto
699 the whole body of the test mice.
700
701 **Fiber photometric recording.** A fiber photometric system (ThinkerTech) was
702 used to record GCaMP signals from *Cbln2*$^{+}$ PF neurons. To induce
703 fluorescence signals, a laser beams from a laser tube (488 nm) was reflected
704 by a dichroic mirror, focused by a 10 × (NA of 0.37) lens and coupled to an
705 optical commutator. A 2-m optical fiber (200 μm in diameter, NA of 0.37) guided
706 the light between the commutator and the implanted optical fiber. To minimize
707 photobleaching, the power intensity at the fiber tip was adjusted to 0.02 mW.
708 The GCaMP7s fluorescence was band-pass filtered (MF525-39, Thorlabs) and
709 collected by a photomultiplier tube (R3896, Hamamatsu). An amplifier (C7319,

710 Hamamatsu) was used to convert the photomultiplier tube current output to
711 voltage signals, which were further filtered through a low-pass filter (40 Hz cut-
712 off; Brownlee 440). The analog voltage signals were digitized at 100 Hz and
713 recorded by a Power 1401 digitizer and Spike2 (CED).

714 AAV-hSyn-DIO-GCaMP7s was stereotacically injected into the PF of
715 Cbln2-IRES-Cre mice followed by the implantation of an optical fiber above the
716 *Cbln2*$^{+}$ PF neurons and the implantation of magnet cylinder inside the dental
717 cement. Three weeks after AAV injection, fiber photometric recording was used
718 to record GCaMP signals from *Cbln2*$^{+}$ PF neurons of free moving mice in the
719 magnetic induction system. A flasing LED triggered by 1s square-wave pluse
720 was simultaneously recorded to synchronize the video, GCaMP signals and the
721 magnetic inducing voltage signals. After the experiments, the optical fiber tip
722 sites in the PF were histologically examined in each mouse.

723

724 **Cell-type-specific RV tracing.** A modified RV-based three-virus system was
725 used for mapping whole-brain inputs to *Cbln2*$^{+}$ PF neurons (Wickersham et al.,
726 2007). All viruses, including AAV2/9-CAG-DIO-EGFP-2A-TVA (5 × 10^{12} viral
727 particles per ml), AAV2/9-CAG-DIO-RVG (5 × 10^{12} viral particles/ml), and EnvA-
728 pseudotyped, glycoprotein (RG)-deleted, and EGFP-expressing RVs (RV-
729 EvnA-ΔG-DsRed) (5.0 × 10^{8} viral particles/ml), were packaged and provided by
730 BrainVTA Inc. (Wuhan, China). A mixture of AAV2/9-CAG-DIO-EGFP-2A-TVA
731 and AAV2/9-CAG-DIO-RVG (1:1, 300 nl) was injected into the PF of Cbln2-
732 IRES-Cre mice unilaterally. Two weeks after AAV helper injection, RV-EvnA-
733 ΔG- DsRed (300 nl) was injected into the same location in the PF of Cbln2-
734 IRES-Cre mice in a biosafety level-2 lab facility. Starter neurons were
735 characterized by the co-expression of DsRed and EGFP, which were restricted
736 in the PF. One week after injection of RV, the mice were perfused with saline,
737 followed by 4% paraformaldehyde (PFA) in phosphate-buffered saline (PBS).
738 The brain was post-fixed in 4% PFA for 8 h and then incubated in PBS
739 containing 30% sucrose until they sank to the bottom. Coronal brain sections
740 (40-μm thickness) were prepared using a cryostat (Leica CM1900). All sections

741 were collected and stained with 4',6-diamidino-2-phenylindole (DAPI). The
742 sections were imaged with an Olympus VS120 epifluorescence microscope
743 (10× objective lens) and analyzed with ImageJ software. For quantification of
744 subregions, boundaries were based on the Allen Institute's reference atlas. We
745 selectively analyzed retrogradely labeled dense areas. The fractional
746 distribution of total cells labeled with RV was measured.
747
748 **Cell-type-specific anterograde tracing.** For cell-type-specific anterograde
749 tracing of *Cbln2*$^{+}$ PF neurons, AAV-DIO-EGFP-syb2 (300 nl) was stereotaxically
750 injected into the PF of Cbln2-IRES-Cre mice. The mice were then maintained
751 in a cage individually. Three weeks after viral injection, mice were perfused with
752 saline followed by 4% PFA in PBS. The brains were post-fixed in 4% PFA for 8
753 hours and then incubated in PBS containing 30% sucrose until they sank to the
754 bottom. Coronal brain sections at 40 μm in thickness were prepared using a
755 cryostat (Leica CM1900). All coronal sections were collected and stained with
756 primary antibody against GFP and DAPI. The coronal brain sections were
757 imaged with an Olympus VS120 epifluorescence microscope (10 × objective
758 lens).
759
760 **Slice physiological recording.** Slice physiological recording was performed
761 according to a previously published protocol. Brain slices containing the PF
762 were prepared from adult mice anesthetized with isoflurane before decapitation.
763 Brains were rapidly removed and placed in ice-cold oxygenated (95% O_2 and
764 5% CO_2) cutting solution (in mM: 228 sucrose, 11 glucose, 26 $NaHCO_3$, 1
765 NaH_2PO_4, 2.5 KCl, 7 $MgSO_4$ and 0.5 $CaCl_2$). Coronal brain slices (400 μm)
766 were cut using a vibratome (VT 1200S, Leica Microsystems). The slices were
767 incubated at 28°C in oxygenated artificial cerebrospinal fluid (ACSF containing
768 in mM: 119 NaCl, 2.5 KCl, 1 NaH_2PO_4, 1.3 $MgSO_4$, 26 $NaHCO_3$, 10 glucose
769 and 2.5 $CaCl_2$) for 30 min, and then kept at room temperature under the same
770 conditions for 1 h before transfer to the recording chamber. The ACSF was
771 perfused at 1ml min^{-1}. The acute brain slices were visualized using a ×40

772 Olympus water immersion lens, differential interference contrast (DIC) optics
773 (Olympus) and a CCD camera. Patch pipettes were pulled from borosilicate
774 glass capillary tubes (Warner Instruments, no. 64-0793) using a PC-10 pipette
775 puller (Narishige). For recording of action potentials (current clamp), pipettes
776 were filled with a solution [in mM: 135 K-methanesulfonate, 10 HEPES buffer,
777 1 EGTA (ethylene glycol tetraacetic acid), 1 Na-GTP, 4 Mg-ATP and 2%
778 neurobiotin (pH7.4)]. The resistance of pipettes varied between 3.0 and 3.5 MΩ.
779 The voltage signals were recorded using MultiClamp 700B and Clampex 10
780 data acquisition software (Molecular Devices). After establishment of the whole-
781 cell configuration and equilibration of the intracellular pipette solution with the
782 cytoplasm, series resistance was compensated to 10-15 MΩ. An optical fiber
783 (200μm in diameter) was used to deliver light pulses, with the fiber tip positioned
784 500 μm above the brain slices. Light-evoked action potentials from ChR2-
785 mCherry^{+} neurons in the PF were triggered by a light-pulse train (473 nm, 2 ms,
786 10 Hz or 20 Hz, 5 mW) synchronized with Clampex 10 data acquisition software
787 (Molecular Devices).
788
789 **Miniscope calcium imaging and data analysis.**
790 1) AAV injection and gradient index (GRIN) lens implantation
791 For miniscope calcium imaging studies, AAV-hsyn-DIO-jGCaMP7s was
792 microinjected into PF of Cbln2-IRES-Cre mice with following coordinates:
793 anterior-posterior, -2.30 mm; medial-lateral, -0.65 mm; dorsal-ventral, -3.2 mm
794 from dura, then the GRIN lens (0.5 mm in diameter × 6.1 mm in length, Inscopix)
795 was implanted 2 weeks after viral injection. For the implantation, the GRIN lens
796 was connected to the imaging system of miniscope to monitor the GCaMP
797 fluorescence during slowly lowering (~100 μm/min) to the target brain area.
798 After the lens was placed at the appropriate coordinates to gain the optimal
799 intensity of GCaMP fluorescence and anchored to the skull with dental cement,
800 the silicon adhesive (Kwik-Sil, WPI) was used to cap the lens to avoid damage.
801 2) Measuring GCaMP fluorescence
802 Miniscope calcium imaging was conducted by using a miniaturized

803 fluorescence microscopy unit (miniscope) linked to a data acquisition device
804 (Inscopix, nVista). At least one day before behavior test and calcium imaging,
805 awake mice with implanted lens were head-fixed on a circular treadmill and a
806 baseplate was implanted above the GRIN lens to get a suitable field for imaging
807 after mounted by the miniscope. Then the miniscope was replaced by a fake
808 one and the mice were returned to their homecages, which enabled the mice
809 to be habituated to the weight of miniscope.
810 On the day of behavior test and calcium imaging, two side-view cameras were
811 used to record the grooming behavior. Synchronization between imaging data
812 and grooming behavior was implemented by the video recording the flash of
813 LED light and a Power 1401 digitizer which was used to mark the signal
814 generated by the data acquisition device when each session of imaging data
815 was documented. Imaging data were acquired at a 20 Hz frame rate.
816 3) Data acquisition and analysis
817 Imaging data were preliminarily processed by the Inscopix data processing
818 software (version 1.6.0). Then the image data were exported as Tiff files. These
819 Tiff files were further analyzed by CNMF-E code in Matlab for the generation of
820 example videos, or manually analyzed by ImageJ software to read the dynamic
821 changes of GCaMP fluorescence frame by frame for each neuron.
822 For the trials which recorded the initial stage of grooming, the frame at which
823 the mice started to groom was denoted as 0 s, and normalized GCaMP
824 fluorescence (ΔF/F) was calculated over a baseline period of -3 s to 0 s.
825 For the trials which recorded the terminate stage of grooming, the frame at
826 which the mice stop grooming was denoted as 0 s, and normalized GCaMP
827 fluorescence (ΔF/F) was calculated over a baseline period of 0 s to 3 s.
828
829 **Immunohistochemistry.** Mice were anesthetized with isoflurane and
830 sequentially perfused with saline and PBS containing 4% PFA. Post-fixation of
831 the brain was avoided to optimize immunohistochemistry. Brains were
832 incubated in PBS containing 30% sucrose until they sank to the bottom.
833 Cryostat sections (40 μm) were collected, incubated overnight with blocking

834 solution (PBS containing 10% goat or donkey serum and 0.7% Triton X-100),
835 and then treated with primary antibodies diluted with blocking solution for 3 - 4
836 h at room temperature. Primary antibodies used for immunohistochemistry are
837 listed in the Supplementary Table 2. Primary antibodies were washed three
838 times with washing buffer (PBS containing 0.7% Triton X-100) before incubation
839 with secondary antibodies (tagged with Alexa Fluor® 488 and Alexa Fluor® 546
840 dilution 1:500; Invitrogen) for 1 h at room temperature. Sections were then
841 washed three times with washing buffer, stained with DAPI, and washed with
842 PBS, transferred onto Super Frost slides, and mounted under glass coverslips
843 with mounting media.
844 Sections were imaged with an Olympus VS120 epifluorescence
845 microscope (10 × objective lens) or a Zeiss LSM 800 confocal microscope (20
846 × and 63 × oil-immersion objective lens). Samples were excited by 405, 488
847 and 561 nm lasers in sequential acquisition mode to avoid signal leakage.
848 Saturation was avoided by monitoring pixel intensity with Hi-Lo mode. Confocal
849 images were analyzed with ImageJ software.
850
851 **RNAscope.** Mice were perfused with PBS treated with 0.1% DEPC (Sigma,
852 D5758), followed by DEPC-treated PBS containing 4% PFA (PBS-PFA). Brains
853 were post-fixed in DEPC-treated PBS-PFA solution overnight and then placed
854 in DEPC-treated 30% sucrose solution at 4°C for 30h. Brain sections to a
855 thickness of 20 μm were prepared using a cryostat (Leica, CM3050S) and
856 subsequently hybridized with the Cbln2 probe (Advanced Cell Diagnostics,
857 428551) following the user manual of the RNAscope kit (Advanced Cell
858 Diagnostics, Doc No. 323100-USM). To visualize the NeuN signals, brain
859 sections were incubated with a primary antibody against NeuN at 4°C for 24 h
860 and then with an Alexa Fluor® 594-conjugated goat anti-rabbit secondary
861 antibody (1:500, A11034, Invitrogen) at room temperature for 2 h. Brain sections
862 were imaged using a Zeiss LSM780 confocal microscope or the Olympus
863 VS120 Slide Scanning System. Detailed information about probe and reagents
864 are listed in the Supplementary Table 2.

865

866 **Data quantification and statistical analyses.** Data collection and analyses
867 were performed blinded to the conditions of the experiments. For statistical
868 analyses of the experimental data, two-sided Student's t-test was used. The "n"
869 used for these analyses represents the number of mice or cells.
870

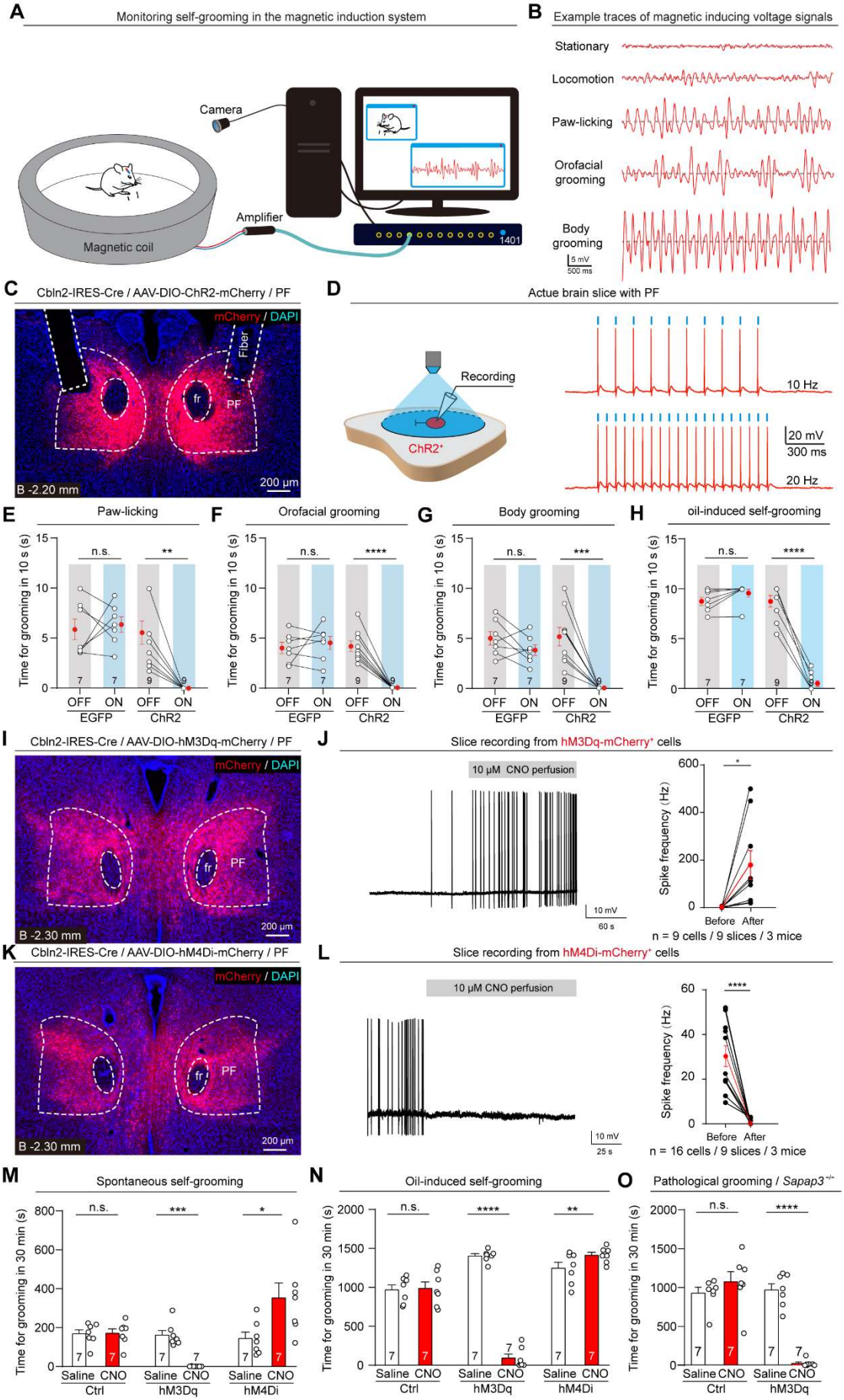
A
Monitoring self-grooming in the magnetic induction system
Camera
Amplifier
Magnetic coil
1401
B
Example traces of magnetic inducing voltage signals
Stationary
Locomotion
Paw-licking
Orofacial grooming
Body grooming
5 mV
500 ms
C
Cbln2-IRES-Cre / AAV-DIO-ChR2-mCherry / PF
mCherry / DAPI
Fiber
fr
PF
B -2.20 mm
200 μm
D
Actue brain slice with PF
Recording
ChR2+
10 Hz
20 mV
300 ms
20 Hz
E
Paw-licking
F
Orofacial grooming
G
Body grooming
H
oil-induced self-grooming
Time for grooming in 10 s (s)
n.s.
**
****
***
OFF
ON
EGFP
ChR2
I
Cbln2-IRES-Cre / AAV-DIO-hM3Dq-mCherry / PF
B -2.30 mm
J
Slice recording from hM3Dq-mCherry+ cells
10 μM CNO perfusion
10 mV
60 s
Spike frequency (Hz)
Before
After
n = 9 cells / 9 slices / 3 mice
K
Cbln2-IRES-Cre / AAV-DIO-hM4Di-mCherry / PF
L
Slice recording from hM4Di-mCherry+ cells
10 μM CNO perfusion
10 mV
25 s
n = 16 cells / 9 slices / 3 mice
M
Spontaneous self-grooming
Time for grooming in 30 min (s)
Saline
CNO
Ctrl
hM3Dq
hM4Di
N
Oil-induced self-grooming
O
Pathological grooming / Sapap3-/-

871

872 **FIG.1 *Cbln2*-expressing PF neurons are essential for self-grooming**
873 (**A**, **B**) Schematic diagram (**A**) and example voltage pulses traces (**B**) showing
874 the magnetic induction system in parallel with a high-speed camera to record
875 the stationary state, locomotion, paw-licking, orofacial grooming and body
876 grooming in mice. (**C**) Example coronal section showing ChR2-mCherry
877 expression in PF of Cbln2-IRES-Cre mice and optical fiber tracks above the PF.
878 (**D**) Light-pulse trains (473 nm, 10 s, 2 mW, 20 Hz / 10 Hz) reliably evoked
879 phase-locked spiking activity in ChR2-mCherry^{+} PF cells. (**E**-**G**) Quantitative
880 analyses of time spent for self-grooming within 10 second before (OFF) and
881 during (ON) photostimulation of *Cbln2*$^{+}$ PF neurons. Photostimulation was
882 conducted when the mice were in the sequential phases of paw-licking (**E**),
883 orofacial grooming (**F**), and body grooming (**G**). (**H**) Quantitative analyses of
884 time spent for oil-induced self-grooming of mice within 10 second before (OFF)
885 and during (ON) photostimulation of *Cbln2*$^{+}$ PF neurons. (**I**) Example coronal
886 section showing bilateral injection of AAV-DIO-hM3Dq-mCherry into the PF of
887 Cbln2-IRES-Cre mice. (**J**) Example trace of action potential firing (left) and
888 quantitative analysis of firing rate (right) showing the effectiveness of CNO to
889 chemogenetically activate hM3Dq-expressing PF neurons in acute brain slices.
890 CNO was dissolved in artificial cerebrospinal fluid (ACSF) (10 μM) and perfused
891 to the brain slices. (**K**) Example coronal section showing bilateral injection of
892 AAV-DIO-hM4Di-mCherry into the PF of Cbln2-IRES-Cre mice. (**L**) Example
893 trace of action potential firing (left) and quantitative analysis of firing rate (right)
894 showing the effectiveness of CNO to chemogenetically silence hM4Di-
895 expressing PF neurons in acute brain slices. CNO was dissolved in artificial
896 cerebrospinal fluid (ACSF) (10 μM) and perfused to the brain slices. (**M-N**)
897 Quantitative analyses of time spent for spontaneous self-grooming (**M**) and oil-
898 induced self-grooming (**N**) within 30 min in mice treated with saline or CNO (1
899 mg/kg) to chemogenetically activate or inactivate *Cbln2*$^{+}$ PF neurons. (**O**)
900 Quantitative analyses of time spent for pathological self-grooming within 30 min
901 in mice treated with saline or CNO (1 mg/kg) to chemogenetically activate
902 *Cbln2*$^{+}$ PF neurons in Cbln2-IRES-Cre / Sapap3$^{-/-}$ mice.
903 Scale bars and numbers of mice are indicated in the graphs. Data in (**E** - **H**),

904 (**J**), (**L**), (**M**) and (**N**) are means ± SEM (error bars). Statistical analyses in (**E** -
905 **H**), (**J**), (**L**), (**M**) and (**N**) were performed using Student's t-test (*$p < 0.05$, **$p <$
906 0.01, ***$p < 0.001$, and ****$p < 0.0001$). For p values, see Supplementary Table
907 1.

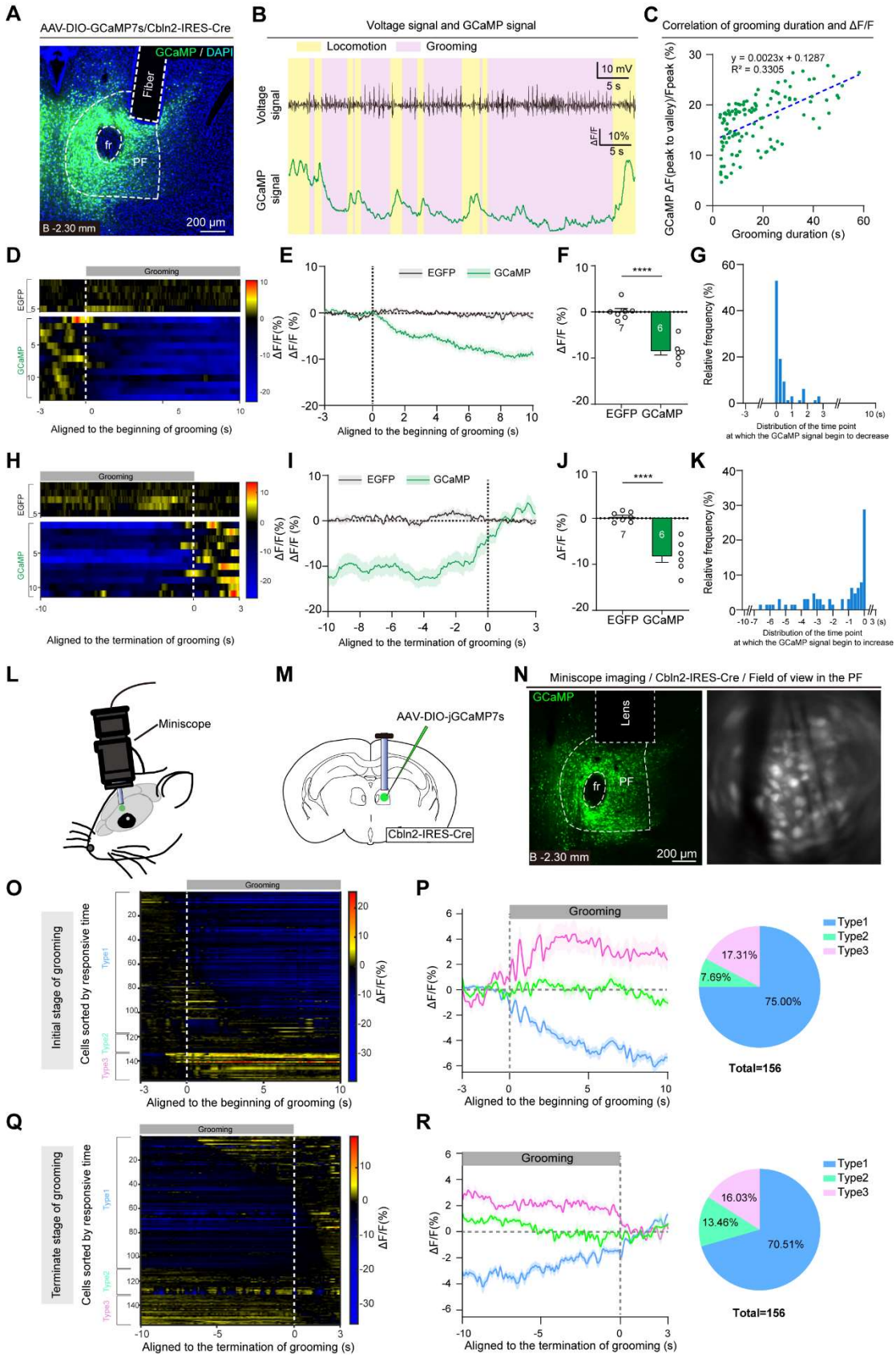
A
AAV-DIO-GCaMP7s/Cbln2-IRES-Cre
GCaMP / DAPI
Fiber
fr
PF
B -2.30 mm
200 μm
B
Voltage signal and GCaMP signal
Locomotion
Grooming
Voltage signal
GCaMP signal
10 mV
5 s
ΔF/F
10%
5 s
C
Correlation of grooming duration and ΔF/F
y = 0.0023x + 0.1287
R² = 0.3305
GCaMP ΔF(peak to valley)/Fpeak (%)
Grooming duration (s)
D
Grooming
EGFP
GCaMP
Aligned to the beginning of grooming (s)
E
EGFP
GCaMP
ΔF/F (%)
Aligned to the beginning of grooming (s)
F
****
ΔF/F (%)
EGFP GCaMP
G
Relative frequency (%)
Distribution of the time point at which the GCaMP signal begin to decrease
H
Grooming
EGFP
GCaMP
Aligned to the termination of grooming (s)
I
EGFP
GCaMP
ΔF/F (%)
Aligned to the termination of grooming (s)
J
****
ΔF/F (%)
EGFP GCaMP
K
Relative frequency (%)
Distribution of the time point at which the GCaMP signal begin to increase
L
Miniscope
M
AAV-DIO-jGCaMP7s
Cbln2-IRES-Cre
N
Miniscope imaging / Cbln2-IRES-Cre / Field of view in the PF
GCaMP
Lens
fr
PF
B -2.30 mm
200 μm
O
Initial stage of grooming
Cells sorted by responsive time
Grooming
Type1
Type2
Type3
ΔF/F(%)
Aligned to the beginning of grooming (s)
P
Grooming
ΔF/F(%)
Aligned to the beginning of grooming (s)
Type1
Type2
Type3
17.31%
7.69%
75.00%
Total=156
Q
Terminate stage of grooming
Cells sorted by responsive time
Grooming
Type1
Type2
Type3
ΔF/F(%)
Aligned to the termination of grooming (s)
R
Grooming
ΔF/F(%)
Aligned to the termination of grooming (s)
Type1
Type2
Type3
16.03%
13.46%
70.51%
Total=156

908

909

910 **FIG.2 *Cbln2*-expressing PF neurons respond to self-grooming**

911 (**A**) Representative micrographs showing the expression of GCaMP7s in PF,
912 and the optical fiber track above the GCaMP$^+$ PF neurons for fiber photometric
913 recording in adult Cbln2-IRES-Cre mice. (**B**) Example GCaMP signals and
914 voltage pulses traces from magnetic induction system in parallel with self-
915 grooming. (**C**) Correlation analysis of average GCaMP7s fluorescence change
916 ($\Delta F_{(peak\text{-}valley)}/F_{peak}$) with grooming duration. (**D**, **H**) Heat-map graphs of
917 GCaMP7s fluorescence of the *Cbln2*$^+$ PF neurons aligned to the onset (**D**) and
918 the offset (**H**) of self-grooming. EGFP were used as control. (**E**, **I**) GCaMP
919 response curve aligned with the initiation (**E**) and termination (**I**) of self-
920 grooming of an example mouse, showing kinetics of GCaMP signal of *Cbln2*$^+$
921 PF neurons. EGFP were used as control. (**F**, **J**) Quantitative analyses of
922 average GCaMP7s fluorescence change (ΔF/F) with the initiation (**F**) and
923 termination (**J**) of self-grooming. (**G**, **K**) Quantitative analyses of distribution of
924 the time point at which the GCaMP signal begin to decrease during the initial
925 stage of grooming (**G**) and increase during the terminate stage of grooming (**H**).
926 (**L**) Schematic diagram showing the schedule for recording GCaMP7s
927 fluorescence from *Cbln2*$^+$ PF single neurons by miniscope. (**M**) Schematic
928 diagram showing viral injection and GRIN lens implantation strategy for calcium
929 imaging of *Cbln2*$^+$ PF neurons. (**N**) Example coronal brain section showing the
930 track of GRIN lens above the GCaMP$^+$ PF neurons in Cbln2-IRES-Cre mice
931 (left). The field of view of raw GCaMP signals (right). (**O**) Heatmaps of the
932 activities (ΔF/F0) in individual PF neurons (n = 6 mice). The vertical white
933 dashed line denotes the grooming behavior onset (0 s). The aligned traces were
934 sorted by the responsive time, and classified to 3 different types depending on
935 the average GCaMP fluorescence intensity difference between the grooming
936 period and the baseline period. Type1: decrease; Type2: no change; Type3:
937 increase. (**P**) Average GCaMP fluorescence response (ΔF/F0) curves of 3
938 different types of neurons aligned with the initiation of grooming behavior (left).
939 Proportion of PF neurons from each category (right, n = 156 neurons from 6
940 mice). (**Q**) Heatmaps of the activities (ΔF/F0) in individual PF neurons (n =6
941 mice). The vertical white dashed line denotes the end of grooming behavior (0

942 s). The aligned traces were sorted by the responsive time, and classified to 3
943 different types depending on the average GCaMP fluorescence intensity
944 difference between the grooming period and the baseline period. Type1:
945 increase; Type2: no change; Type3: decrease. (**R**) Average fluorescence
946 response (ΔF/F0) curves of 3 different types of neurons aligned with the
947 termination of grooming behavior (left). Proportion of PF neurons from each
948 category (right, n = 156 neurons from 6 mice).
949 Scale bars and numbers of mice are indicated in the graphs. Data in (**E**, **F**) and
950 (**I**, **J**) are means ± SEM (error bars). Statistical analyses in (**F**) and (**J**) were
951 performed using Student's t-test (****p < 0.0001). For p values, see
952 Supplementary Table 1.
953

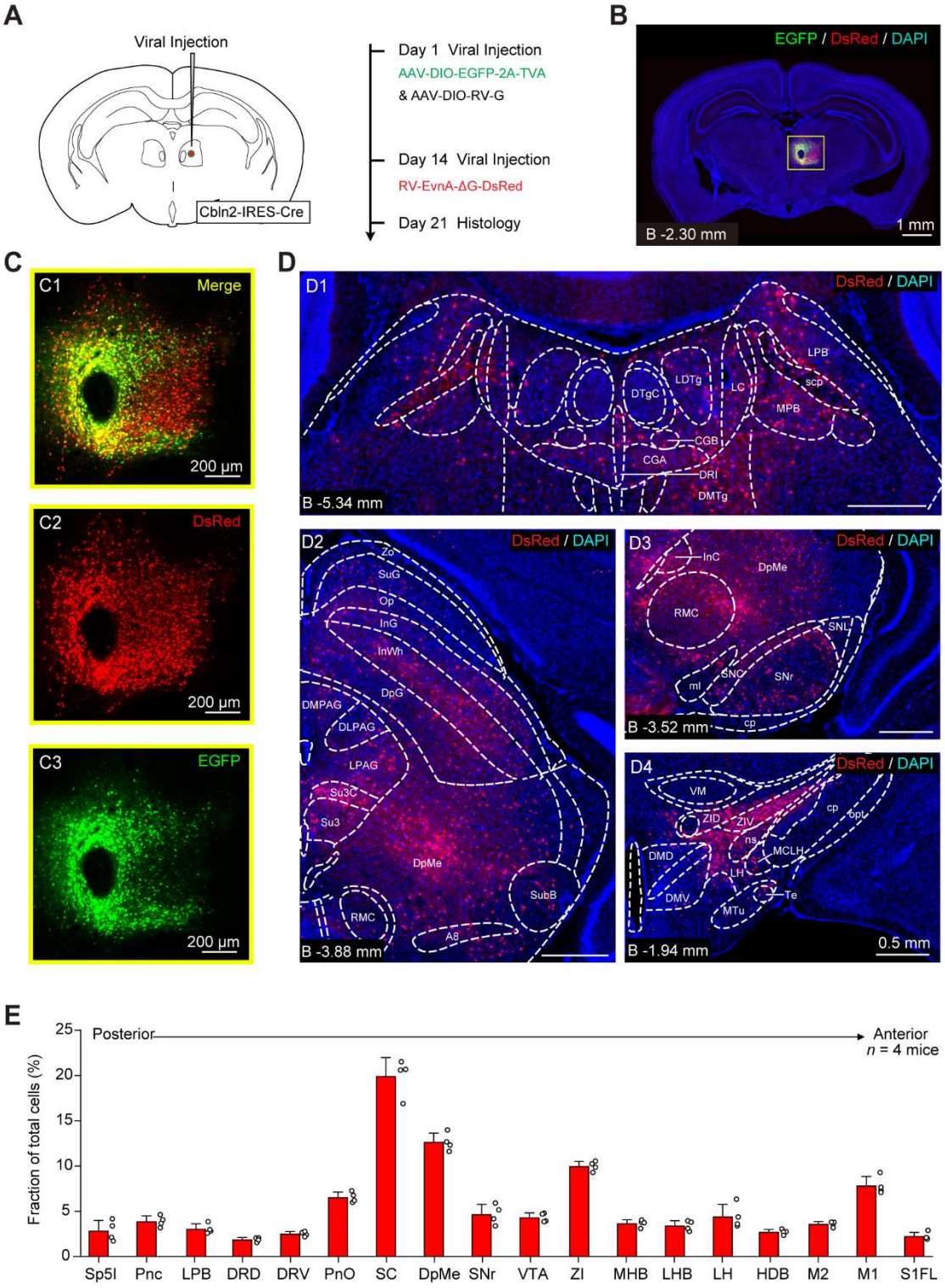
A
Viral Injection
Cbln2-IRES-Cre
Day 1 Viral Injection
AAV-DIO-EGFP-2A-TVA
& AAV-DIO-RV-G
Day 14 Viral Injection
RV-EvnA-ΔG-DsRed
Day 21 Histology
B
EGFP / DsRed / DAPI
B -2.30 mm
1 mm
C
C1
Merge
200 µm
C2
DsRed
200 µm
C3
EGFP
200 µm
D
D1
DsRed / DAPI
LPB
scp
LDTg
LC
DTgC
MPB
CGB
CGA
DRI
DMTg
B -5.34 mm
D2
DsRed / DAPI
Zo
SuG
Op
InG
InWh
DpG
DMPAG
DLPAG
LPAG
Su3C
Su3
DpMe
SubB
RMC
A8
B -3.88 mm
D3
DsRed / DAPI
InC
DpMe
RMC
SNL
SNC
SNr
ml
cp
B -3.52 mm
D4
DsRed / DAPI
VM
ZID
ZIV
cp
opt
ns
MCLH
DMD
LH
DMV
Te
MTu
B -1.94 mm
0.5 mm
E
Posterior
Anterior
n = 4 mice
Fraction of total cells (%)
25
20
15
10
5
0
Sp5I
Pnc
LPB
DRD
DRV
PnO
SC
DpMe
SNr
VTA
ZI
MHB
LHB
LH
HDB
M2
M1
S1FL

954

955 **FIG.3 Retrograde tracing of *Cbln2*$^+$ PF neurons with RV**

956 (**A**) Schematic diagram showing the viral injection strategy for the retrograde
957 tracing of *Cbln2*$^+$ PF neurons using a combination of AAV and rabies virus (RV).
958 (**B**-**C**) Representative coronal section showing that the viral injection center, as
959 indicated by the co-expression of EGFP and DsRed, was localized in the PF.
960 Note that the double-labeled cells indicate starter cells (**C**). (**D**) Example
961 micrographs showing DsRed$^+$ cells in different brain regions, including the LPB
962 (D1), the SC (D2), the SNr (D3) and the ZI (D4). (**E**) Fraction of total RV-labeled
963 cells in different brain regions monosynaptically projecting to the *Cbln2*$^+$ PF
964 neurons. Note that data in (**E**) were normalized by dividing the total number of
965 DsRed+ cells in these brain regions. Numbers of mice (**E**) are indicated in the
966 graphs.

967 Scale bars are labeled in the graphs. Data in (**E**) are means ± SEM (error bars).
968 The experiment (**B**-**D**) was repeated four times independently with similar
969 results.

970

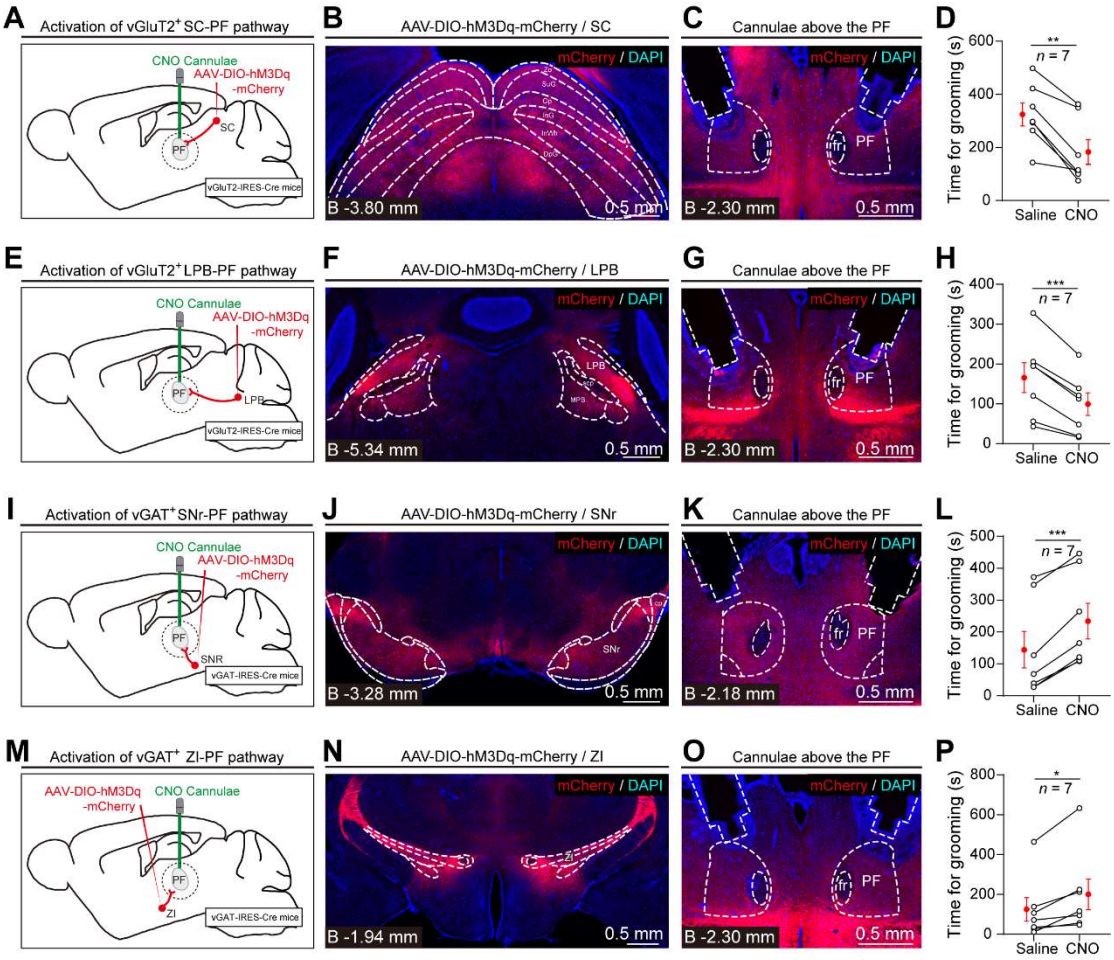
A
Activation of vGluT2+ SC-PF pathway
CNO Cannulae
AAV-DIO-hM3Dq -mCherry
SC
PF
vGluT2-IRES-Cre mice
B
AAV-DIO-hM3Dq-mCherry / SC
mCherry / DAPI
B -3.80 mm
0.5 mm
C
Cannulae above the PF
mCherry / DAPI
PF
fr
B -2.30 mm
0.5 mm
D
Time for grooming (s)
n = 7
Saline
CNO
E
Activation of vGluT2+ LPB-PF pathway
CNO Cannulae
AAV-DIO-hM3Dq -mCherry
LPB
PF
vGluT2-IRES-Cre mice
F
AAV-DIO-hM3Dq-mCherry / LPB
mCherry / DAPI
B -5.34 mm
0.5 mm
G
Cannulae above the PF
mCherry / DAPI
PF
fr
B -2.30 mm
0.5 mm
H
Time for grooming (s)
n = 7
Saline
CNO
I
Activation of vGAT+ SNr-PF pathway
CNO Cannulae
AAV-DIO-hM3Dq -mCherry
SNR
PF
vGAT-IRES-Cre mice
J
AAV-DIO-hM3Dq-mCherry / SNr
mCherry / DAPI
SNr
B -3.28 mm
0.5 mm
K
Cannulae above the PF
mCherry / DAPI
PF
fr
B -2.18 mm
0.5 mm
L
Time for grooming (s)
n = 7
Saline
CNO
M
Activation of vGAT+ ZI-PF pathway
AAV-DIO-hM3Dq -mCherry
CNO Cannulae
ZI
PF
vGAT-IRES-Cre mice
N
AAV-DIO-hM3Dq-mCherry / ZI
mCherry / DAPI
ZI
B -1.94 mm
0.5 mm
O
Cannulae above the PF
mCherry / DAPI
PF
fr
B -2.30 mm
0.5 mm
P
Time for grooming (s)
n = 7
Saline
CNO

971

972 **FIG.4 *Cbln2*$^+$ PF input pathways involvement in self-grooming**

973 (**A, E**) Schematic diagram showing the injection of AAV-DIO-hM3Dq-mCherry
974 into the SC or LPB of vGluT2-IRES-Cre mice, followed by cannulae
975 implantation above the PF to enable cell-type-specific activation of the vGluT2$^+$
976 SC-PF pathway (**A**) or vGluT2$^+$ LPB-PF pathway (**E**). (**B-C, F-G**) Example
977 micrographs showing hM3Dq-mCherry expression in the SC (**B**) or LPB (**F**) and
978 the cannulae above hM3Dq-mCherry$^+$ axon terminals in the PF (**C**, **G**). (**D, H**)
979 Quantitative analyses of time spent for spontaneous self-grooming within 30
980 minutes in mice infused with saline or CNO to chemogenetically activate
981 vGluT2$^+$ SC-PF pathway (**D**) or vGluT2$^+$ LPB-PF pathway (**H**). (**I, M**) Schematic
982 diagram showing the injection of AAV-DIO-hM3Dq-mCherry into the SNr or ZI
983 of vGAT-IRES-Cre mice, followed by cannulae implantation above the PF to
984 enable cell-type-specific activation of the vGAT$^+$ SNr-PF pathway (**I**) or vGAT$^+$
985 ZI–PF pathway (**M**). (**J-K**, **N-O**) Example micrographs showing hM3Dq-
986 mCherry expression in the SNr (**J**) or ZI (**N**) and the cannulae above hM3Dq-
987 mCherry$^+$ axon terminals in the PF (**K**, **O**). (**L, P**) Quantitative analyses of time
988 spent for spontaneous self-grooming within 30 minutes in mice infused with
989 saline or CNO to chemogenetically activate vGAT$^+$ SNr-PF pathway (**L**) or
990 vGAT$^+$ ZI-PF pathway (**P**).

991 Scale bars and numbers of mice are indicated in the graphs. Data in (**D**), (**H**),
992 (**L**), and (**P**) are means ± SEM (error bars). Statistical analyses in (**D**), (**H**), (**L**),
993 and (**P**) were performed using Student's t-test (*$p < 0.05$, **$p < 0.01$, and ***$p <$
994 0.001). For p values, see Supplementary Table 1.

995

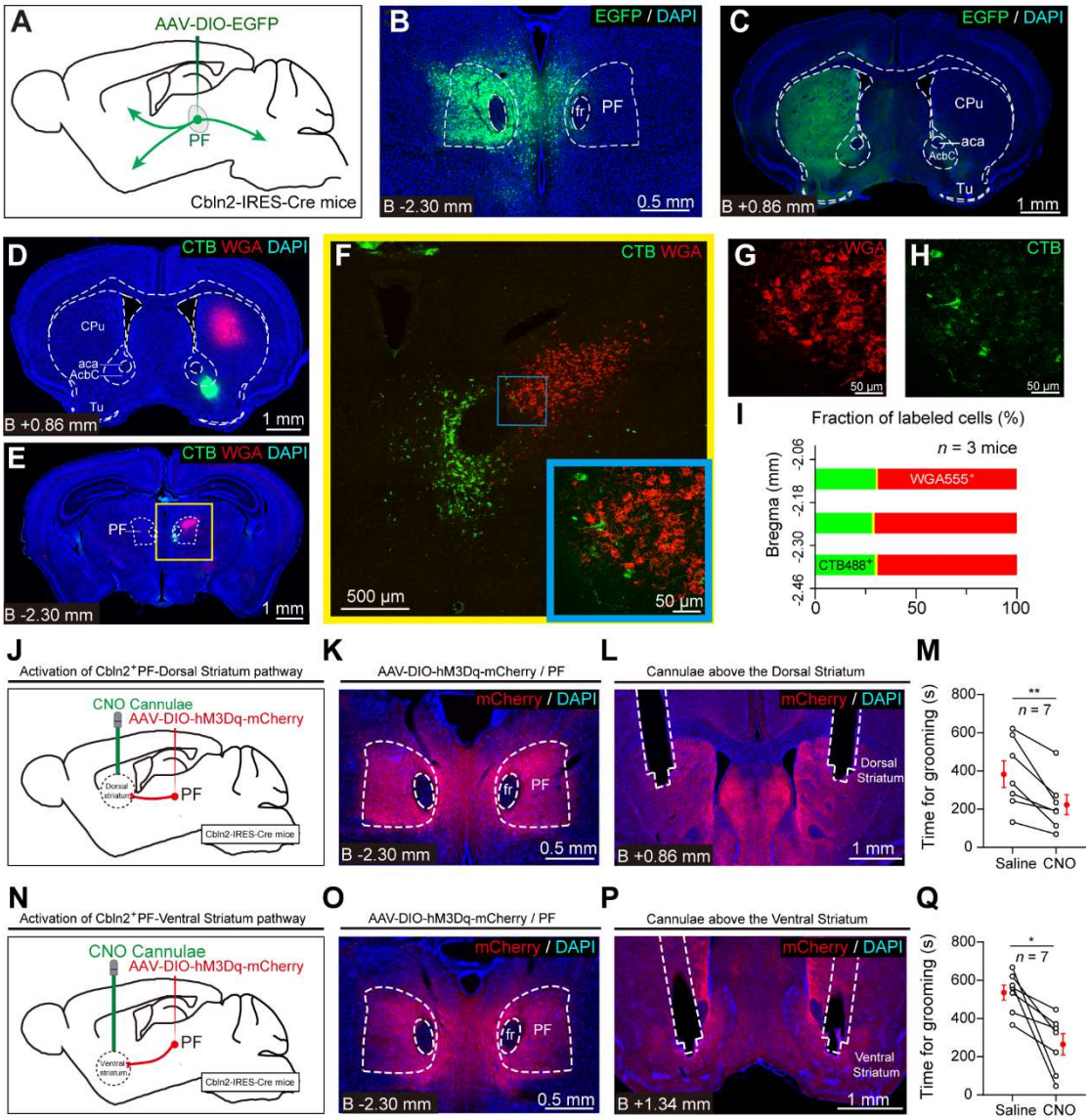
A
AAV-DIO-EGFP
PF
Cbln2-IRES-Cre mice
B
EGFP / DAPI
fr
PF
B -2.30 mm
0.5 mm
C
EGFP / DAPI
CPu
aca
AcbC
Tu
B +0.86 mm
1 mm
D
CTB WGA DAPI
CPu
aca
AcbC
Tu
B +0.86 mm
1 mm
E
CTB WGA DAPI
PF
B -2.30 mm
1 mm
F
CTB WGA
500 µm
50 µm
G
WGA
50 µm
H
CTB
50 µm
I
Fraction of labeled cells (%)
n = 3 mice
Bregma (mm)
-2.06
-2.18
-2.30
-2.46
WGA555+
CTB488+
0
50
100
J
Activation of Cbln2+PF-Dorsal Striatum pathway
CNO Cannulae
AAV-DIO-hM3Dq-mCherry
Dorsal striatum
PF
Cbln2-IRES-Cre mice
K
AAV-DIO-hM3Dq-mCherry / PF
mCherry / DAPI
fr
PF
B -2.30 mm
0.5 mm
L
Cannulae above the Dorsal Striatum
mCherry / DAPI
Dorsal Striatum
B +0.86 mm
1 mm
M
Time for grooming (s)
800
600
400
200
0
**
n = 7
Saline
CNO
N
Activation of Cbln2+PF-Ventral Striatum pathway
CNO Cannulae
AAV-DIO-hM3Dq-mCherry
Ventral striatum
PF
Cbln2-IRES-Cre mice
O
AAV-DIO-hM3Dq-mCherry / PF
mCherry / DAPI
fr
PF
B -2.30 mm
0.5 mm
P
Cannulae above the Ventral Striatum
mCherry / DAPI
Ventral Striatum
B +1.34 mm
1 mm
Q
Time for grooming (s)
800
600
400
200
0
*
n = 7
Saline
CNO

998 **FIG.5 The role of *Cbln2*$^+$ PF–striatum pathway in self-grooming**

999 (**A**) Schematic diagram showing the viral injection strategy for labeling *Cbln2*$^+$
1000 PF neurons using AAV-DIO-ChR2-mCherry in adult Cbln2-IRES-Cre mice. (**B-**
1001 **C**) Representative micrographs from the PF showing EGFP expression in the
1002 PF neurons (**B**) and EGFP-positive axon terminals in the striatum (**C**). (**D**)
1003 Retrograde labelling of PF neurons by injecting WGA555 into dorsal striatum
1004 and CTB488 into ventral striatum. (**E-H**) Example coronal brain sections
1005 showing dorsal striatum-projecting WGA$^+$ PF neurons and ventral striatum-
1006 projecting CTB+ neurons. (**I**) Quantitative analyses reflecting the overlap
1007 between dorsal striatum- and ventral striatum-projecting PF neurons within
1008 different bregmas, showing that dorsal striatum- projecting and ventral striatum-
1009 projecting *Cbln2*$^+$ PF neurons are largely segregated. (**J, N**) Schematic diagram
1010 showing the injection of AAV-DIO-hM3Dq-mCherry into the PF of Cbln2-IRES-
1011 Cre mice, followed by cannulae implantation above the dorsal striatum or
1012 ventral striatum to enable cell-type-specific activation of the *Cbln2*$^+$ PF-dorsal
1013 striatum pathway (**J**) or *Cbln2*$^+$ PF-ventral striatum pathway (**N**). (**K-L, O-P**)
1014 Example micrographs showing hM3Dq-mCherry expression in the PF (**K**, **O**)
1015 and the cannulae above hM3Dq-mCherry$^+$ axon terminals in the dorsal striatum
1016 (**L**) or ventral striatum (**P**). (**M**, **Q**) Quantitative analyses of time spent for
1017 spontaneous self-grooming within 30 minutes in mice infused with saline or
1018 CNO to chemogenetically activate *Cbln2*$^+$ PF-dorsal striatum pathway (**M**) or
1019 *Cbln2*$^+$ PF-ventral striatum (**Q**).

1020 Scale bars and numbers of mice are indicated in the graphs. Data in (**M**) and
1021 (**Q**) are means ± SEM (error bars). Statistical analyses (**M** and **Q**) were
1022 performed using Student's t-test (*$p < 0.05$, and **$p < 0.01$). For p values, see
1023 Supplementary Table 1.

1024

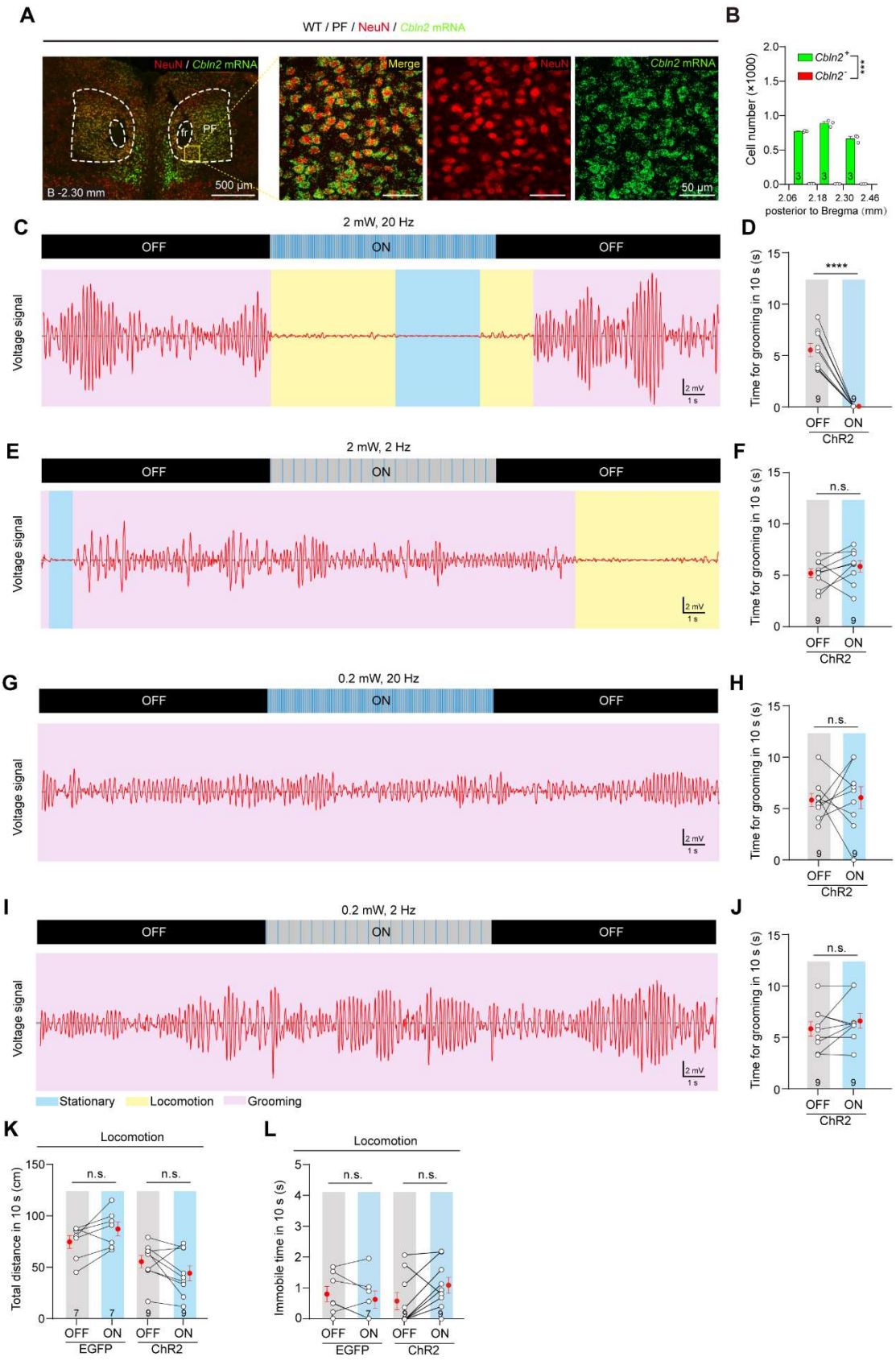
A
WT / PF / NeuN / Cbln2 mRNA
NeuN / Cbln2 mRNA
Merge
NeuN
Cbln2 mRNA
PF
fr
B -2.30 mm
500 μm
50 μm
B
Cbln2+
Cbln2-
***
Cell number (×1000)
posterior to Bregma (mm)
C
2 mW, 20 Hz
OFF
ON
OFF
Voltage signal
2 mV
1 s
D
****
Time for grooming in 10 s (s)
OFF
ON
ChR2
E
2 mW, 2 Hz
F
n.s.
G
0.2 mW, 20 Hz
H
I
0.2 mW, 2 Hz
J
Stationary
Locomotion
Grooming
K
Locomotion
Total distance in 10 s (cm)
EGFP
ChR2
L
Immobile time in 10 s (s)

1025

1026 **sFIG.1 Photostimulation of *Cbln2*$^{+}$ PF neurons inhibit spontaneous self-**
1027 **grooming but locomotion.**
1028 (**A**) Example micrographs showing the distributions of *cbln2* mRNA in the PF
1029 of WT mice. (**B**) Quantitative analyses of number of PF cells expressing *cbln2*
1030 mRNA
1031 (green) in coronal sections, as indicated by the distance to bregma. (**C, E, G, I**)
1032 Example voltage pulses traces showing the magnetic induction system in
1033 parallel with a high-speed camera to record spontaneous self-grooming, within
1034 10 second before (OFF) and during (ON) photostimulation of *Cbln2*$^{+}$ PF
1035 neurons by various light-pulse trains (473 nm, 2 ms, 2 mW, 20 Hz) for (**C**),
1036 (473 nm, 2 ms, 2 mW, 2 Hz) for (**D**), (473 nm, 2 ms, 0.2 mW, 20 Hz) for (**G**), and
1037 (473 nm, 2 ms, 0.2 mW, 2 Hz) for (**I**). (**D, F, H, J**) Quantitative analyses of of time
1038 spent for spontaneous self-grooming within 10 seconds before (OFF) and
1039 during (ON) photostimulation of *Cbln2*$^{+}$ PF neurons by various light-pulse trains
1040 (473 nm, 2 ms, 2 mW, 20 Hz) for (D), (473 nm, 2 ms, 2 mW, 2 Hz) for (F),
1041 (473 nm, 2 ms, 0.2 mW, 20 Hz) for (H), and (473 nm, 2 ms, 0.2 mW, 2 Hz) for (**J**).
1042 (**K**, **L**) Quantitative analyses of time for total distance (L) and immobile time (L)
1043 of mice within 10 seconds before (OFF) and during (ON) photostimulation of
1044 *Cbln2*$^{+}$ PF neurons.
1045 Scale bars are labeled in the graphs. Numbers of mice are indicated in the
1046 graphs (**B**, **D**, **F**, **H**, **J**, **K** and **L**). Data in (**B**), (**D**), (**F**), (**H**), (**J**), (**K**) and (**L**) are
1047 means ± SEM (error bars). Statistical analyses in (**B**), (**D**), (**F**), (**H**), (**J**), (**K**) and
1048 (**L**) were performed using Student's t-test (***$p < 0.001$, and ****$p < 0.0001$).
1049

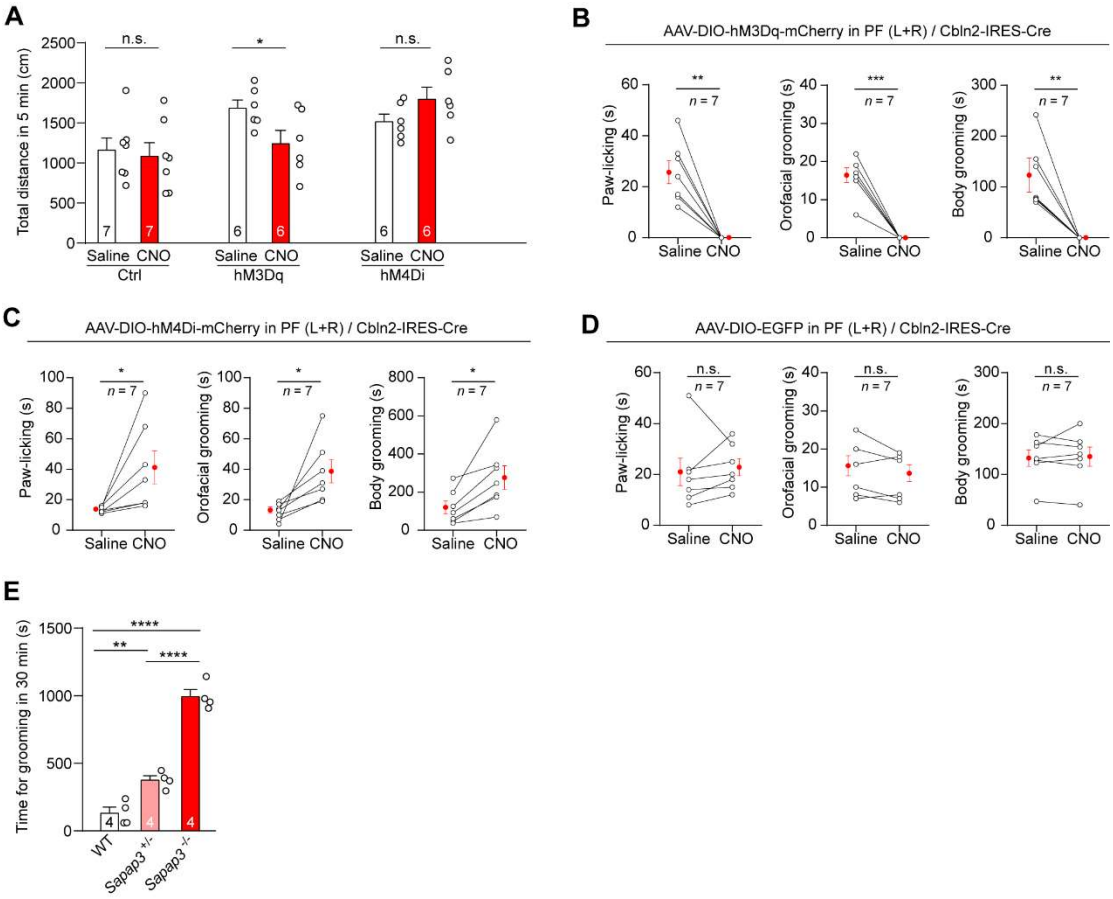
A
Total distance in 5 min (cm)
n.s.
*
n.s.
Saline CNO
Ctrl
hM3Dq
hM4Di
B
AAV-DIO-hM3Dq-mCherry in PF (L+R) / Cbln2-IRES-Cre
Paw-licking (s)
Orofacial grooming (s)
Body grooming (s)
n = 7
C
AAV-DIO-hM4Di-mCherry in PF (L+R) / Cbln2-IRES-Cre
D
AAV-DIO-EGFP in PF (L+R) / Cbln2-IRES-Cre
E
Time for grooming in 30 min (s)
WT
Sapap3 +/-
Sapap3 -/-

1050

1051 **sFIG.2 Chemogenetic activation of Cbln2$^+$ PF neurons inhibit paw-licking,**
1052 **orofacial grooming and body grooming. (A)** Quantitative analyses of total
1053 distance within 5 minutes in mice treated with saline or CNO (1 mg/kg) to
1054 chemogenetically activate or inactivate *Cbln2*$^+$ PF neurons. (**B**) Injection of
1055 AAV-DIO-hM3Dq-mCherry into PF of Cbln2-IRES-Cre mice, quantitative
1056 analyses of time spent for paw-licking, orofacial grooming, and body grooming
1057 of mice within 30 minutes treated with saline or CNO (1 mg/kg) to
1058 chemogenetically activate *Cbln2*$^+$ PF neurons. (**C**) Injection of AAV-DIO-hM4Di-
1059 mCherry into PF of Cbln2-IRES-Cre mice, quantitative analyses of time spent
1060 for paw-licking, orofacial grooming, and body grooming of mice within 30
1061 minutes treated with saline or CNO (1 mg/kg) to chemogenetically inactivate
1062 *Cbln2*$^+$ PF neurons. (**D**) Injection of AAV-DIO-EYFP into PF of Cbln2-IRES-Cre
1063 mice, quantitative analyses of time spent for paw-licking, orofacial grooming,
1064 and body grooming of mice within 30 minutes treated with saline or CNO (1
1065 mg/kg). (**E**) Quantitative analyses of time spent for excessive self-grooming
1066 within 30 minutes in *Sapap3*$^{+/-}$ and *Sapap3*$^{-/-}$ mice.
1067 Numbers of mice are indicated in the graphs (**A**-**E**). Data in (**A**-**E**) are means ±
1068 SEM (error bars). Statistical analyses in (**A**-**E**) were performed using Student's
1069 t-test (*$p < 0.05$, **$p < 0.01$, ***$p < 0.001$, and ****$p < 0.0001$).
1070

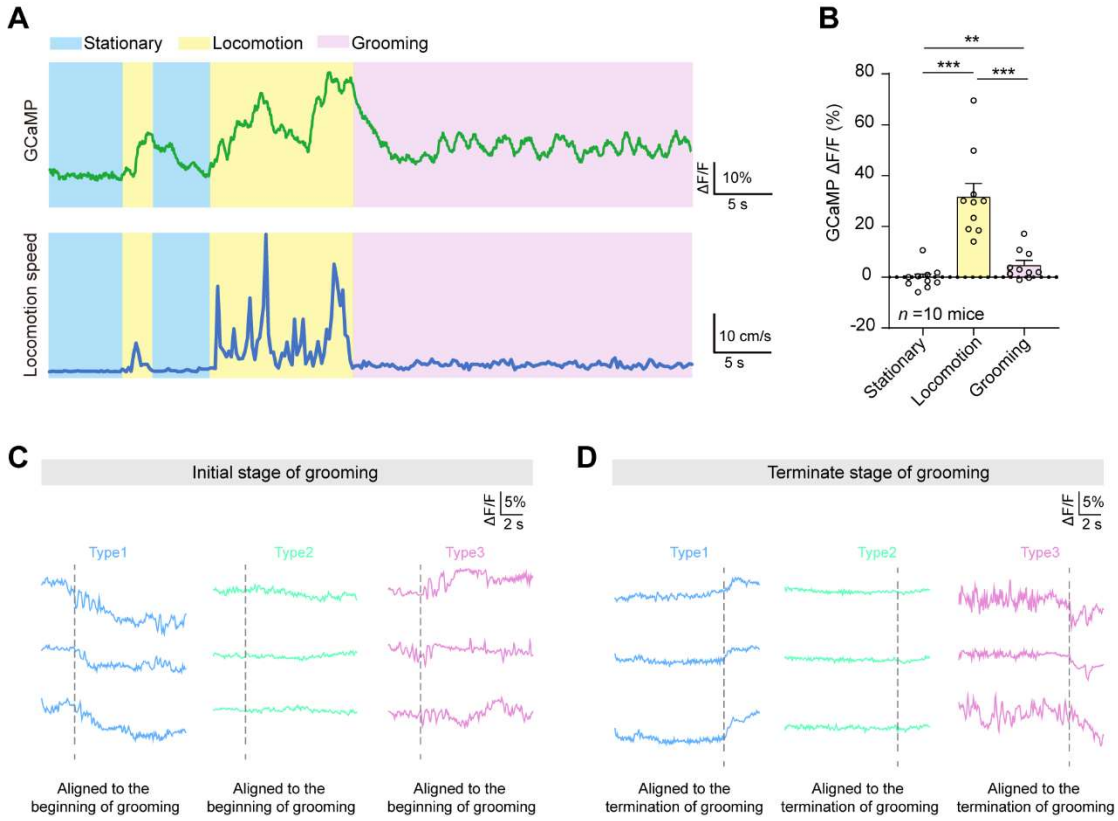
A
Stationary
Locomotion
Grooming
GCaMP
ΔF/F
10%
5 s
Locomotion speed
10 cm/s
5 s
B
GCaMP ΔF/F (%)
80
60
40
20
0
-20
**
***
***
n =10 mice
Stationary
Locomotion
Grooming
C
Initial stage of grooming
ΔF/F
5%
2 s
Type1
Type2
Type3
Aligned to the beginning of grooming
Aligned to the beginning of grooming
Aligned to the beginning of grooming
D
Terminate stage of grooming
ΔF/F
5%
2 s
Type1
Type2
Type3
Aligned to the termination of grooming
Aligned to the termination of grooming
Aligned to the termination of grooming

1071

1072 **sFIG.3 Cbln2-expressing PF neurons show decreased during self-**
1073 **grooming**
1074 (**A**) Example GCaMP signals from *Cbln2*$^{+}$ PF neurons during the stationary,
1075 locomotion, and self-grooming stages by fiber photometric recording. (**B**)
1076 Quantitative analyses of average GCaMP7s fluorescence change (ΔF/F) with
1077 during the stationary, locomotion, and self-grooming stages. (**C**) Representative
1078 GCaMP response curve from single *Cbln2*$^{+}$ PF neurons aligned with the
1079 initiation of self-grooming. (**D**) Representative GCaMP response curve from
1080 single *Cbln2*$^{+}$ PF neurons aligned with the termination of self-grooming.
1081 Numbers of mice are indicated in the graphs (**B**). Data in (**B**) are means ± SEM
1082 (error bars). Statistical analyses in (**B**) were performed using Student's t-test
1083 (**$p < 0.01$, and ***$p < 0.001$).
1084

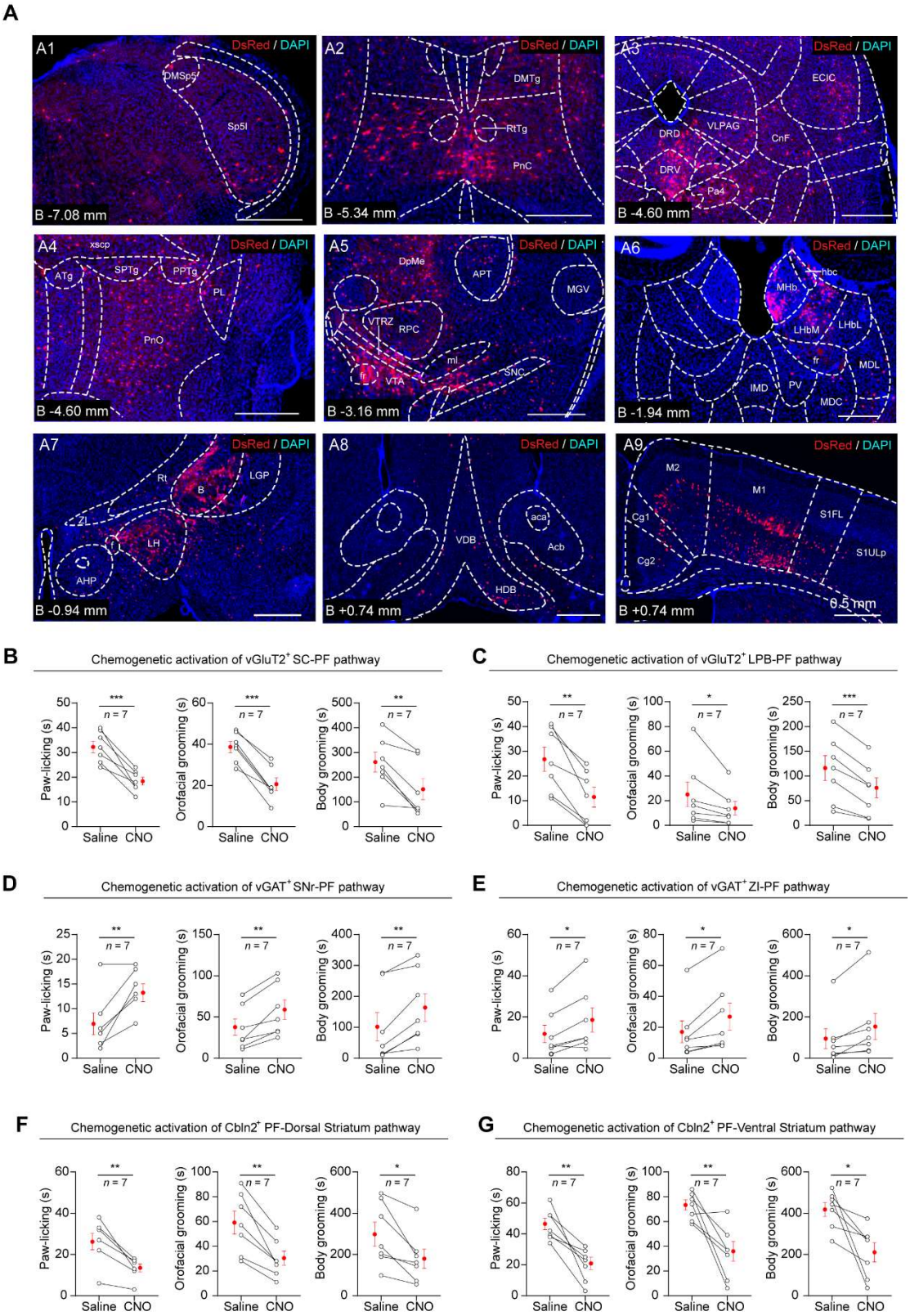
A
A1
DsRed / DAPI
DMSp5
Sp5I
B -7.08 mm
A2
DMTg
RtTg
PnC
B -5.34 mm
A3
ECIC
DRD
VLPAG
CnF
DRV
Pa4
B -4.60 mm
A4
xscp
ATg
SPTg
PPTg
PL
PnO
B -4.60 mm
A5
DpMe
APT
MGV
VTRZ
RPC
ml
SNC
fr
VTA
B -3.16 mm
A6
hbc
MHb
LHbM
LHbL
fr
MDL
IMD
PV
MDC
B -1.94 mm
A7
Rt
B
LGP
ZL
LH
AHP
B -0.94 mm
A8
aca
VDB
Acb
HDB
B +0.74 mm
A9
M2
M1
Cg1
S1FL
S1ULp
Cg2
0.5 mm
B +0.74 mm
B
Chemogenetic activation of vGluT2+ SC-PF pathway
C
Chemogenetic activation of vGluT2+ LPB-PF pathway
D
Chemogenetic activation of vGAT+ SNr-PF pathway
E
Chemogenetic activation of vGAT+ ZI-PF pathway
F
Chemogenetic activation of Cbln2+ PF-Dorsal Striatum pathway
G
Chemogenetic activation of Cbln2+ PF-Ventral Striatum pathway
Paw-licking (s)
Orofacial grooming (s)
Body grooming (s)
n = 7
Saline
CNO

1085

1086 **sFIG.4 Chemogenetic activation of input pathway of *Cbln2*$^+$ PF neurons**
1087 **inhibit paw-licking, orofacial grooming and body grooming**
1088 **(A)** Example micrographs showing DsRed$^+$ cells in different brain regions,
1089 including the Sp5I (A1), the Pnc (A2), the DRD (A3), the DRV (A3), the PnO
1090 (A4), the VTA (A5), the MHb (A6), the LH (A7), the HDB (A8), the M1 (A9) and
1091 the M2 (A9). Scale bars are labeled in the graphs. Number of mice: four. Data
1092 in E are presented as mean ± SEM.Scale bars are labeled in the graphs.
1093 Numbers of mice are indicated in the graphs (**B**-**G**). Quantitative analyses of
1094 time spent for paw-licking, orofacial grooming and body grooming within 30
1095 minutes in mice infusused with saline or CNO to chemogenetically activate
1096 vGluT2$^+$ SC-PF pathway (**B**), vGluT2$^+$ LPB-PF pathway (**C**) vGAT$^+$ SNr-PF
1097 pathway (**D**), vGAT$^+$ ZI-PF pathway (**E**), *Cbln2*$^+$ PF-dorsal striatum pathway (**F**)
1098 or *Cbln2*$^+$ PF-ventral striatum pathway (**G**). Data in (**B**-**G**) are means ± SEM
1099 (error bars). Statistical analyses in (**B**-**G**) were performed using Student's t-test
1100 (*$p < 0.05$, **$p < 0.01$, and ***$p < 0.001$).
1101

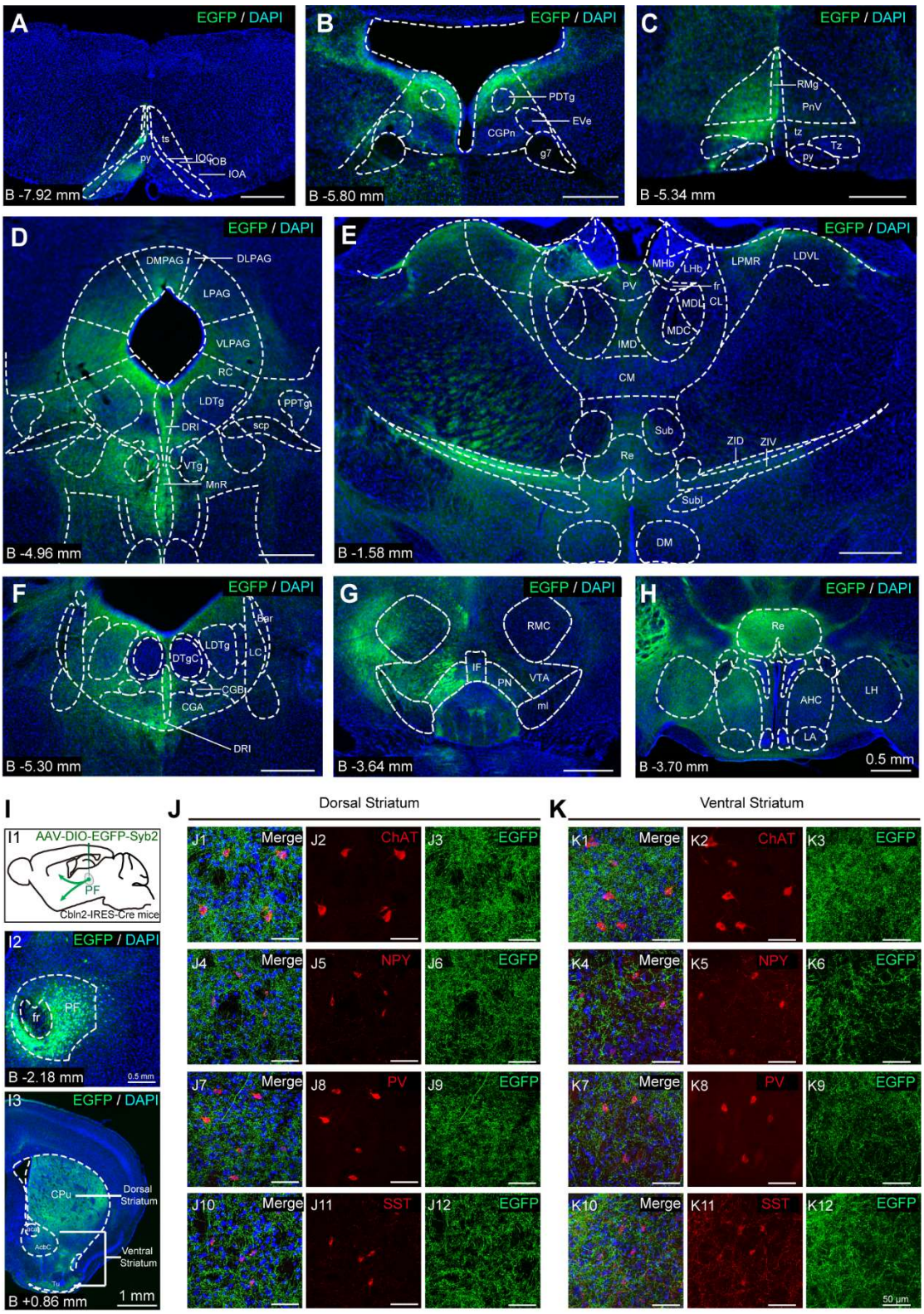
A
EGFP / DAPI
ts
py
IOC
IOB
IOA
B -7.92 mm
B
EGFP / DAPI
PDTg
EVe
CGPn
g7
B -5.80 mm
C
EGFP / DAPI
RMg
PnV
tz
Tz
py
B -5.34 mm
D
EGFP / DAPI
DMPAG
DLPAG
LPAG
VLPAG
RC
LDTg
PPTg
DRI
scp
VTg
MnR
B -4.96 mm
E
EGFP / DAPI
MHb
LHb
LPMR
LDVL
PV
fr
MDL
CL
MDC
IMD
CM
Sub
ZID
ZIV
Re
Subl
DM
B -1.58 mm
F
EGFP / DAPI
Per
LDTg
DTgC
LC
CGBl
CGA
DRI
B -5.30 mm
G
EGFP / DAPI
RMC
IF
PN
VTA
ml
B -3.64 mm
H
EGFP / DAPI
Re
AHC
LH
LA
B -3.70 mm
0.5 mm
I
I1
AAV-DIO-EGFP-Syb2
PF
Cbln2-IRES-Cre mice
I2
EGFP / DAPI
PF
fr
B -2.18 mm
0.5 mm
I3
EGFP / DAPI
CPu
Dorsal Striatum
Ventral Striatum
B +0.86 mm
1 mm
J
Dorsal Striatum
J1 Merge
J2 ChAT
J3 EGFP
J4 Merge
J5 NPY
J6 EGFP
J7 Merge
J8 PV
J9 EGFP
J10 Merge
J11 SST
J12 EGFP
K
Ventral Striatum
K1 Merge
K2 ChAT
K3 EGFP
K4 Merge
K5 NPY
K6 EGFP
K7 Merge
K8 PV
K9 EGFP
K10 Merge
K11 SST
K12 EGFP
50 µm

1102

1103 **sFIG.5 Mapping the monosynaptic outputs of *Cbln2*$^{+}$ PF neurons**

1104 (**A**-**H**) Example coronal brain sections showing EGFP^{+} synaptic terminals of
1105 *Cbln2*$^{+}$ PF neurons in the target brain regions, including the py (**A**), CGPn (**B**),
1106 PnV (**C**), LPAG (**D**), VLPAG (**D**), DRI (**D**), MnR (**D**), ZI (**E**), LC (**F**), CGA (**F**),
1107 LDTg (**F**), VTA (**G**), Re (**H**), AHC (**H**), and LH (**H**). (**I**) Antrograde labeling of
1108 synaptic terminals of Cbln2+ PF neurons in the dorsal and ventral striatum. (**J**
1109 and **K**) Various subtypes of interneurons, including ChAT^{+}, NPY^{+}, PV^{+} and SST^{+}
1110 neurons in the dorsal stratum (**J**) and ventral stratum (**K**) were surrounded by
1111 the EGFP^{+} synaptic terminals from *Cbln2*$^{+}$ PF neurons.

1112 Scale bars are labeled in the graphs.

1113